
**ROYAL INSTITUTE**
**OF TECHNOLOGY**

# Recovering Moho parameters using gravimetric and seismic data

**Majid Abrehdary**

**Doctoral Dissertation in Geodesy**

**Division of Geodesy and Satellite Positioning**
**Department of Urban Planning and Environment**
**Royal Institute of Technology (KTH)**

**SE-100 44 Stockholm**
**Sweden**

**April 2016**

TRITA SOM 2016-02
ISSN 1654-2754
ISNR KTH/SoM/2016-02/SE
ISBN 978-91-7595-879-8

Majid Abrehdary: Recovering Moho parameters using gravimetric and seismic data

Main supervisor:
Professor Lars Erik Sjöberg

Co-supervisor:
Docent Mohammad Bagherbandi

Faculty Opponent:
Professor Pavel Novák
Department of Mathematics University of West Bohemia Univerzitní 22 306 14 Pilsen, Czech Republic

Evaluation committee:
Dr. Jonas Ågren, Division of Geodesy, Lantmäteriet, Gävle, Sweden
Associate professor Björn Lund, Department of Earth Sciences, Uppsala University
Professor Hossein Nahavandchi, Norwegian University of Science and Technology, Department of Civil and Transport Engineering, Trondheim, Norway



Printed by

Universitetsservice US-AB, Drottning Kristinas väg 53B, SE-100 44 Stockholm, Sweden

# Abstract

Isostasy is a key concept in geoscience to interpret the state of mass balance between the Earth's crust and mantle. There are four well-known isostatic models: the classical models of Airy/Heiskanen (A/H), Pratt/Hayford (P/H), and Vening Meinesz (VM) and the modern model of Vening Meinesz-Moritz (VMM). The first three models assume a local and regional isostatic compensation, whereas the latter one supposes a global isostatic compensation scheme.

A more satisfactory test of isostasy is to determine the Moho interface. The Moho discontinuity (or Moho) is the surface, which marks the boundary between the Earth's crust and upper mantle. Generally, the Moho interface can be mapped accurately by seismic observations, but limited coverage of seismic data and economic considerations make gravimetric or combined gravimetric-seismic methods a more realistic technique for imaging the Moho interface either regional or global scales.

It is the main purpose of this dissertation to investigate an isostatic model with respect to its feasibility to use in recovering the Moho parameters (i.e. Moho depth and Moho density contrast). The study is mostly limited to the VMM model and to the combined approach on regional and global scales. The thesis briefly includes various investigations with the following specific subjects:

1) to investigate the applicability and quality of satellite altimetry data (i.e. marine gravity data) in Moho determination over the oceans using the VMM model, 2) to investigate the need for methodologies using gravimetric data jointly with seismic data (i.e. combined approach) to estimate both the Moho depth and Moho density contrast over regional and global scales, 3) to investigate the spherical terrain correction and its effect on the VMM Moho determination, 4) to investigate the residual isostatic topography (RIT, i.e. difference between actual topography and isostatic topography) and its effect in the VMM Moho estimation, 5) to investigate the application of the lithospheric thermal-pressure correction and its effect on the Moho

geometry using the VMM model, 6) Finally, the thesis ends with the application of the classical isostatic models for predicting the geoid height.

The main input data used in the VMM model for a Moho recovery is the gravity anomaly/disturbance corrected for the gravitational contributions of mass density variation due in different layers of the Earth's crust (i.e. stripping gravity corrections) and for the gravity contribution from deeper masses below the crust (i.e. non-isostatic effects). The corrections are computed using the recent seismic crustal model CRUST1.0.

Our numerical investigations presented in this thesis demonstrate that 1) the VMM approach is applicable for estimating Moho geometry using a global marine gravity field derived by satellite altimetry and that the possible mean dynamic topography in the marine gravity model does not significantly affect the Moho determination, 2) the combined approach could help in filling-in the gaps in the seismic models and it also provides good fit to other global and regional models more than 90 per cent of the locations, 3) despite the fact that the lateral variation of the crustal depth is rather smooth, the terrain affects the Moho result most significantly in many areas, 4) the application of the RIT correction improves the agreement of our Moho result with some published global Moho models, 5) the application of the lithospheric thermal-pressure correction improves the agreement of VMM Moho model with some other global Moho models, 6) the geoid height cannot be successfully represented by the classical models due to many other gravitational signals from various mass variations within the Earth that affects the geoid.

**Key words:** crust, gravity, mantle, Moho depth, non-isostatic effect, residual isostatic topography, stripping, thermal state, Vening Meinesz-Moritz model.

## Dedication

*To my beloved father and mother,*

*Mahmoud and Batoul*

# Acknowledgements

First and foremost, I would like to express my sincerest gratitude and thanks to my main supervisor, Professor Lars Erik Sjöberg, for his guidance, support and encouragement during the course of this study. I am indebted to him for his valuable comments, scientific rigor and continuous engagement. Without his knowledge, experience and open mind, this thesis would never have seen the light of day.

I would like to express my heartfelt gratitude to my co-supervisor, Docent Mohammad Bagherbandi for his guidance, valuable discussions and thorough comments. His contribution in programming is greatly appreciated. Without his constant help this thesis would not have been possible.

I would like to thank my colleagues at the Division of Geodesy and Satellite Positioning especially Mr. Asenjo, Professor Jensen, Dr. Fan, Docent Horemuz, Dr. Jansson, Professor Eshagh, Dr. Shirazian, Dr. Zhao, Dr. Ssengendo, Mr. Alizadeh and present PhD students.

My thanks also go to my former teachers and my nearest friends in Iran: Associate professor Kiamehr, Dr. Lari, Dr. Sadatipour, Morteza, Ala, Amir and Reza who encouraged me to continue my education to PhD level.

Funding for this research was provided by the Swedish National Space Board (SNSB) and private University of North Tehran. This research could not be completed without this support.

I would like to dedicate this thesis to all of my family especially to my beloved Father, Mother and younger sister and her husband for their emotional support, patience and understanding over my PhD studies.

Stockholm, April 2016

Majid Abrehdary

# Table of Contents

Abstract ..... i
Dedication ..... iii
Acknowledgements ..... iv
List of Tables ..... ix
List of Figures ..... x
List of Abbreviations ..... xi
**PART ONE** ..... 1
**1. Introduction** ..... 1
1.1 Earth's structure ..... 1
1.2 Isostasy and its modelling ..... 2
1.3 Background of the Moho modelling ..... 3
1.4 Research objectives and author's contributions ..... 6
1.4.1 Research objectives ..... 6
1.4.2 Contents of Part one ..... 8
1.4.3 Contents of Part two ..... 8
**2. Moho parameter determination based on gravimetric and seismic methods** ..... 11
2.1 The classical isostatic models ..... 11
2.1.1 The Airy/Heiskanen model ..... 11
2.1.2 The Pratt-Hayford model ..... 12
2.1.3 The Vening Meinesz regional model ..... 13
2.2 The Vening Meinesz-Moritz model ..... 13
2.2.1 Main concept of the VMM hypothesis ..... 14
2.2.2 New definitions of Bouguer and isostatic gravity anomalies ..... 15
2.2.3 The VMM solution by the refined Bouguer gravity disturbance ..... 16
2.2.3.1 The VMM Moho depth ..... 17
2.2.3.2 The VMM Moho Density Contrast ..... 18
2.3 Seismic methods ..... 19
2.3.1 Principle of the Methods ..... 19
2.4 The global Earth crustal model ..... 20

2.4.1 The gravimetric models ..... 20
2.4.1.1 DMM2.0 ..... 20
2.4.1.2 GEMMA1.0 ..... 21
2.4.2. The seismological models ..... 21
2.4.2.1 CRUST1.0 ..... 21
2.4.2.2 MDN07 ..... 22
2.4.3 Combining the gravimetric and seismological models ..... 22
2.4.3.1 KTH11C ..... 22
2.4.3.2 GEMMA2012C ..... 22
2.5 Uncertainties in the Moho parameters ..... 22
2.5.1 Uncertainties in the VMM model ..... 23
2.5.2 Uncertainties in the seismic crustal model ..... 24
2.6. Numerical investigations ..... 25
2.6.1 Uncertainties in the VMM and CRUST1.0 models ..... 30
**3. Additive corrections to gravity disturbance** ..... 33
3.1 Crust density variation corrections ..... 33
3.2 Non-Isostatic Effects ..... 34
3.3. Numerical investigations ..... 36
**4. The combined approach** ..... 39
4.1 Combining the gravimetric and seismic models ..... 39
4.2. Numerical investigations ..... 40
**5. Conclusions and Future Research** ..... 45
5.1 Conclusions ..... 45
5.2 Future research ..... 47
**Bibliography** ..... 49
**PART TWO-PUBLICATIONS** ..... 55

## PAPER A:

Abrehdary, M., Sjöberg, L.E., and Bagherbandi, M. (2015). Modelling Moho depth in ocean areas based on satellite altimetry using Vening Meinesz–Moritz' method, (Published in Journal of Acta Geodaetica et Geophysica, 1-13).

**PAPER B:**

Abrehdary, M., Sjöberg, L.E., and Bagherbandi, M. (2015). Combined Moho parameters determination using CRUST1.0 and Vening Meinesz-Moritz Model, (Published in Journal of Earth Science, 26(4), 607-616).

**PAPER C:**

Abrehdary, M., Sjöberg, L.E., and Bagherbandi, M. (2015). The spherical terrain correction and its effect on the gravimetric-isostatic Moho determination, (Published in Geophysical Journal International, 204(1), 262-273).

**PAPER D:**

Abrehdary, M., Sjöberg, L.E., Bagherbandi, M., and Sampietro D. (2015) Modelling Moho parameters and their uncertainties from the combination of the seismic and satellite gravity data, (Submitted to Journal of Geodesy).

**PAPER E:**

Bagherbandi, M., Sjöberg, L.E., Tenzer, R., and Abrehdary, M. (2015). A new Fennoscandian crustal thickness model based on CRUST1.0 and a gravimetric–isostatic approach, (Published in Journal of Earth-Science Reviews, 145, 132-145).

**PAPER F:**

Bagherbandi, M., Tenzer, R., Sjöberg, L.E., and Abrehdary, M. (2015). On the residual isostatic topography effect in the gravimetric Moho determination, (Published in Journal of Geodynamics, 83, 28-36).

**PAPER G:**

Bagherbandi, M., Sjöberg, L.E., Bai, Y., Tenzer, R., Abrehdary, M. Miranda, S., and Sanchez, J.M. (2016). Effect of the lithospheric thermal state on the Moho geometry, (Submitted to Journal of South American Earth Science).

**PAPER H:**

Sjöberg, L.E., Abrehdary, M., and Bagherbandi, M. (2014). The observed geoid height versus Airy's and Pratt's isostatic models using matched asymptotic expansions, (Published in Journal of Acta Geodaetica et Geophysica, 49(4), 473-490).

# List of Tables

**Table 2.1.** Statistics of the Bouguer gravity disturbance and Moho depth computed through satellite altimetry. ..... 25

**Table 2.2.** Statistics of global estimates of the Bouguer gravity disturbance and Moho depth. ..... 27

**Table 2.3.** Statistics of global estimates of the CRUST1.0 and VMM standard errors for 1°×1° block data ..... 31

**Table 3.1.** Statistics of global estimates of the gravity disturbances, stripping gravity corrections and non-isostatic effects ..... 37

**Table 4.1.** Statistics of global estimates of the combined approach for 1°×1° block data. ..... 41

**Table 4.2.** Sources of regional Moho depth models used in this study ..... 43

# List of Figures

**Figure 2.1. (a)** The Bouguer gravity (in mGal) disturbance generated by satellite altimetry, and **(b)** The Moho depth (in km) estimated via satellite altimetry ..... 26

**Figure 2.2. (a)** The estimated simple spherical Bouguer gravity disturbance corrected for the bathymetry, ice, sediment and non-isostatic effects (unit mGal), and **(b)** The estimated refined spherical Bouguer gravity disturbance (unit mGal) corrected for the bathymetry, ice, sediment and non-isostatic effects. ..... 29

**Figure 2.3. (a)** The estimated VMM Moho depth based on the simple spherical Bouguer gravity disturbance, and **(b)** The estimated VMM Moho depth based on the refined spherical Bouguer gravity disturbance (in km).. 29

**Figure 2.4. (a)** The MDC derived by the CRUST1.0 model, and **(b)** standard errors of the MDC ..... 31

**Figure 3.1. (a)** The free-air gravity disturbance computed using the GOCO03S coefficients complete to degree 180 of spherical harmonics, **(b)** The topographic gravity correction, **(c)** The bathymetric stripping gravity correction, **(d)** The ice density variation stripping gravity correction, **(e)** The sediments density variation stripping gravity corrections, **(f)** non-isostatic effects and **(g)** refined Bouguer gravity disturbances after applying the topographic and stripping gravity corrections due to the ocean, ice, sediment density variations and non-isostatic effects (unit mGal) ..... 38

**Figure 4.1. (a)** The Moho depth estimated from combined approach, and **(b)** standard errors of the estimated Moho depth (unit km) ..... 41

**Figure 4.2. (a)** The MDC estimated by combined approach, and **(b)** standard errors of the MDC (unit $kg/m^3$) ..... 42

**Figure 4.3. (a)** Regional map of seismic estimates of the Moho depth used in this study (in km), and **(b)** Coherence between combined approach and Moho depths from seismic regional models. ..... 44

# List of Abbreviations

| | |
|---|---|
| A/H | Airy/Heiskanen |
| CHAMP | CHAllenging Minisatellite Payload |
| CRUST1.0 | Crustal thickness model with resolution 1°×1° |
| CRUST2.0 | Crustal thickness model with resolution 2°×2° |
| DTM | Digital Terrain Model |
| DMM2.0 | Delft Moho Model with resolution 2°×2° |
| EGM | Earth Gravitational Model |
| GEEMA | GOCE Exploitation for Moho Modeling and Applications |
| GRACE | Gravity Recovery And Climate Experiment |
| GOCE | Gravity field and steady-state Ocean Circulation Explorer |
| MDC | Moho Density Contrast |
| MDN07 | Mixture Density Network 2007 |
| Moho | Mohorovičić discontinuity |
| MSE | Mean Square Error |
| NIE | Non-Isostatic Effect |
| P/H | Pratt/Hayford |
| PREM | Preliminary Reference Earth Model |
| RIT | Residual Isostatic Topography |
| RMS | Root Mean Square |
| VMM | Vening Meinesz-Moritz |
| VM | Vening Meinesz |

# PART ONE

## Chapter 1

*''Since the $\overline{P}$ wave can only reach down to a depth of 50 km, this depth marks the limit of the upper layer of the earth's crust. At this surface, there must be a sudden change of the material which makes up the interior of the earth, because there a step in the velocity of the seismic waves must exist.''*

(*Andrija Mohorovičić, 1910*)

# 1. Introduction

### 1.1 Earth's structure

Generally, the structure of the Earth's interior can be layered in three main concentric shells by their different physical and chemical properties. The first layer is the crust, which is the outermost and thinnest layer. The crust can be categorized into the oceanic and continental crust. The oceanic crust ranges from 5-10 km thick, while the continental crust ranges from 35-70 km thick. The layer below the crust is the mantle, which is the thickest layer of the Earth. It can be divided into the upper and lower mantle. The upper mantle extends from the crust to a depth of 660 km and the lower mantle extends from 660-2900 km beneath the Earth's surface. The innermost layer of the Earth is the core, which can be classified into the outer and inner core. The outer core varies from 2900-5100 km in depth, whereas the inner core varies from 5100-6400 km below the Earth's surface (see Anderson, 1989).

The geoscientists typically use three sources of information to figure out the interior of the Earth's structure:

The first set is understood by direct evidence from rock samples by drilling projects. In this way, the scientists attempt to drill holes in the Earth's surface, to a maximum depth of about 12 km, and explode

rocks for inferring the conditions within the Earth's interior. The drilling method is severely limited, because it is difficult to drill a deep hole due to the high pressure and temperature, and on the other hand it is a time-consuming and expensive technology (Kearey et al. 2013).

The second set includes the records of seismic waves, which are generated, for example, by earthquakes, explosions, volcanoes and other natural sources. Accordingly, specialists can detect information about the Earth's interior through detailed analysis of seismic data. This information can reveal that Earth consists of three main layers, the crust, the mantle, and the core. At this point it deserves to be mentioned that the seismic data are also expensive to collect and therefore sparse and in-homogeneously distributed around the Earth (see Anderson, 1989).

The third set of information in modeling the Earth's interior is the gravity field models generated through the modern satellite gravity missions such as Challenging Mini-satellite Payload (CHAMP), Gravity Recovery and Climate Experiment (GRACE) and Gravity field and steady state Ocean Circulation Explorer (GOCE), which can provide a global and homogeneous coverage of data. A huge improvement can also be obtained in the accuracy and spatial resolution of these models by combining them with airborne and ground-based gravity data and satellite altimetry data (see Hamayun, 2014).

### 1.2 Isostasy and its modelling

Isostasy is a vital concept in the Earth sciences describing the state of equilibrium (or mass balance) to which the mantle tends to balance the mass of the crust in the absence of external disturbing forces. The transport of material over the Earth's surface, such as glaciers, volcanism, and sedimentation could be factors that disturb isostasy (see Sjöberg and Bagherbandi, 2014).

Isostasy can be viewed as an alternative to Archimedes' principle of hydrostatic equilibrium, which states that a lighter solid body floats on

the denser underlying fluid like ice cubes in water. ‘’*When a certain area of the crust reaches the state of isostasy, it is said to be in isostatic equilibrium (or balance), and the depth at which isostatic equilibrium prevails is called the compensation depth’’* (see Sjöberg and Bagherbandi, 2014).

The four principle models of isostasy can briefly be listed as (a) the Airy/Heiskanen (A/H; Airy 1855; Heiskanen 1924 and 1938), (b) the Pratt/Hayford (P/H; Pratt 1855; Hayford 1909), (c) the Vening Meinesz (VM; Meinesz 1931), and (d) the Vening Meinesz-Moritz (VMM; Moritz 1990; Sjöberg 2009), respectively.

A/H and P/H are local models in which variations in topographic height are compensated by either changes in the thickness of a uniform crustal density or by lateral changes in density of the crust and mantle. Both models predict that the crust and mantle respond to loads (e.g. volcanoes) or unloads (e.g. erosion) locally, while disregarding neighbouring regions in their presumptions (see Watts, 2011). However, due to the elasticity of the Earth this is not a very realistic assumption. Vening Meinesz (1931) modified the A/H isostatic theory and introduced a regional model, in which loads and unloads are balanced by a gentle bending or flexure over a broad area. Moritz (1990) generalized the VM model from a regional to a global compensation with a spherical sea level approximation, as expressed by Sjöberg (2009) in mathematical form.

### 1.3 Background of the Moho modelling

One of the primary interfaces of the Earth’s interior is the boundary between the Earth’s crust and mantle, which is called the Mohorovičić discontinuity (or Moho). The discontinuity was first discovered in 1909 by Croatian seismologist Andrija Mohorovičić, when analyzing seismograph records of an earthquake in the Kapula valley, namely P-waves (compressional waves) and S-waves (shear waves). He noticed that the P-waves, which travel deeper into the Earth, moved faster than those that travel nearer the surface. Accordingly, he concluded that the Earth is not homogeneous, and at a specific depth there must be a

boundary surface, which distinguishes two media with different compositions, and by which the seismic waves propagate with different velocities (see Hamayun, 2014).

Currently the Moho interface can be studied using two main methods: the gravimetric and seismic ones. These methods cannot provide the same results, as they are based on different hypotheses, different types, qualities and spatial distributions of data (Sjöberg, 2009).

Seismic methods are one of the major techniques in modelling the thickness of the Earth's crust, where the base of the crust is defined as the Moho. Moho models based on seismic data can be locally very accurate but useless in areas without adequate seismic observations, particularly over large portions of the oceans. Also the seismic data acquisition is costly with lack of global coverage. In contrast, while using satellite gravity data, information on the Moho can be inferred from a uniform and global data set. However, Moho models based on gravity data are in general characterized by simplified hypotheses to guarantee the uniqueness of the solution of the inverse gravitational problem (see Sjöberg and Bagherbandi, 2011; Reguzzoni et al. 2013). In any case, due to the complementary information described above, a combined gravimetric-seismic method could be useful in modelling the Moho.

Much research using seismic surveys for recovering Moho has been carried out in the last decades globally. For instance, Shapiro and Ritzwoller (2002) and Meier et al. (2007) compiled global Moho models based on seismic data analysis, and Lebedev et al. (2013) estimated the Moho depth using seismic surface waves. For global studies the most frequently used crustal models are the CRUST2.0 (Bassin et al. 2000) and CRUST1.0 model (Laske et al. 2013), compiled with 2°×2° and 1°×1° resolutions, respectively.

Over large areas of the world with a sparse coverage of seismic data, a gravimetric-isostatic or combined gravimetric/seismic method can be useful. For example, Vening Meinesz (1931) modified the Airy/Heiskanen theory (Heiskanen and Moritz 1967, Section 3.4) by

introducing a regional isostatic compensation model based on a thin plate lithospheric flexure model (Watts, 2001, p. 114). Moritz (1990, Section 8) generalized the Vening Meinesz hypothesis from a regional to global compensation. Sjöberg (2009) expressed the Vening Meinesz-Moritz (VMM) problem as that of solving a non-linear Fredholm integral equation, and he also presented some solutions for recovering the Moho depth. The VMM method was also followed up by some additional theoretical studies, such as methods for estimating the Moho density contrast (MDC) (Sjöberg and Bagherbandi, 2011) and for reducing the Bouguer gravity anomaly for non-isostatic effects (Bagherbandi and Sjöberg, 2012; Bagherbandi et al. 2013). Tenzer and Bagherbandi (2012) demonstrated that the Moho depth estimated from the isostatic gravity disturbance based on solving the VMM model has a better agreement with the CRUST2.0 seismic model than those computed by the isostatic gravity anomaly. Their argument was also theoretically explained by Sjöberg (2013). Reguzzoni et al (2013) estimated the Moho depth and MDC using the combination of the CRUST2.0 and a GOCE global gravity models. Tenzer and Chen (2014) applied a new method to estimate the Moho depth using the gravimetric forward and inverse modeling in the spectral domain. Hamayun (2014) produced a Moho depth model using gravity disturbances together with two seismic models. Tenzer et al. (2015a) applied the CRUST1.0 model to estimate the average densities of crustal structures, and to compile the gravity field quantities derived by the Earth's crustal structures and to investigate their spatial and spectral characteristics and their correlation with the crustal geometry in context of the gravimetric Moho determination. Sjöberg et al. (2015) showed that the application of the Bouguer gravity disturbances and the no-topography in VMM model to determine the Moho depth provide very similar results, implying the importance of not using the traditional Bouguer gravity anomaly for gravity inversion. Tenzer et al. (2015b) formulated the gravimetric inverse problem for determination of Moho geometry based on adopting the generalized compensation model by considering the variable depth and density of compensation. Reguzzoni and Sampietro (2015)

presented a new procedure applied to GOCE data for estimating the new crustal model GEMMA.

## 1.4 Research objectives and author's contributions

### *1.4.1 Research objectives*

The study of the Moho structure can supply very useful information for applications in geology, geophysics and geodesy. For example, it is especially important in investigating the dynamics of the Earth's interior, in unraveling the gravitational signal of anomalous subsurface distribution and in determining the geoid or quasi-geoid.

The Moho parameter determination can generally be achieved through two techniques: the seismic and gravimetric ones. The seismic observations utilized in compiling global Moho models are typically sparse, and therefore the interpolation of global Moho depths, particularly over areas without adequate seismic data, could yield unrealistic results with large uncertainties. Accordingly, over large parts of the world with a limited coverage of seismic data, the gravimetric or combination of seismic and gravimetric data (combined approach) is fruitfully offered.

Up to now, several different isostatic models have been proposed for mapping the Moho depth and MDC, and it is not specified which model is most suitable, which makes it difficult to judge what is the best method in a certain situation. The simplest isostatic models are the classical ones, with a local and regional compensation. In any case, there is no doubt that the VMM model with a global isostatic compensation is the most realistic gravimetric-isostatic method.

In this thesis the used methods of determining Moho parameters can differ with respect to other proposed methods in different ways.

In general, one main distinction is to apply the VMM isostatic model of the Moho. As the VMM hypothesis (in contrast to the classical isostatic hypotheses) is based on a global isostatic compensation, each compensated topographic mass column will experience a mass

anomaly versus that of the classical models (which are fully compensated locally or regionally).

One can also distinguish our method from other methods for mapping the Moho surface from the used gravity anomaly or disturbance observations. For instance, the simple or refined Bouguer gravity anomaly versus the simple or refined Bouguer gravity disturbance.

In gravimetric studies the anomalous density structure not only within the crust but necessarily within the whole lithosphere should be modeled. Hence, the observed gravity data should be corrected in two main ways namely for the gravitational contributions of mass density variations due in different layers of the Earth's crust such as ice and sediments, as well as for the gravity contribution from deeper masses below the crust.

Another distinction is to combine the seismic and gravimetric models to diminish the seismic data gaps (i.e. combined approach), an approach which has not been very common in previous studies.

Another feature is to compute the Moho depth and MDC uncertainties due to errors of the VMM and seismic models, which are typically overlooked. A proper understanding of these errors is necessary to secure the quality of the Moho results.

The main objective of this thesis is to recover the Moho parameters (i.e. Moho depth and MDC) using available gravimetric and seismic models over regional and global scales to a resolution of 1°×1°. Particularly, this study has its main emphasis on the Moho parameter determination based on the VMM and combined methods.

The gravimetric-isostatic VMM Moho determination comprises of two steps: the first step is the gravimetric forward modelling, and the other one is the gravimetric inverse modelling.

Before using gravity data for Moho inversion, they should be corrected due to the gravitational contributions of known anomalous crustal density structures, mainly density variations of oceans, glacial ice, and sediments (i.e. stripping gravity corrections). For this purpose,

the gravimetric forward modeling technique is first used to compute the stripping gravity corrections using the recent seismic crustal model CRUST1.0. Moreover, the gravity signal associated with deeper masses below the crust (i.e. non-isostatic effects) must also be removed. The gravimetric inverse problem is then defined using the non-linear Fredholm integral equation of the first kind to determine the Moho depth (Sjöberg, 2009).

In addition, we apply a combined approach to simultaneously estimate Moho depth and MDC by the VMM and available seismic models like CRUST1.0 (Laske et al. 2013) and MDN07 (Meier et al. 2007) models. This approach should have an optimal choice of the variance-covariance matrix of observations for solving the system of normal equations.

### *1.4.2 Contents of Part one*

Chapter 1 starts with introducing and explaining the general scope of the thesis. In Chapters 2 and 3 we review the mathematical aspects of the VMM model to determine the Moho depth and MDC, including its additive corrections (i.e. stripping gravity corrections and non-isostatic effects). In Chapter 4 we explain our technique of combining the gravimetric and seismic data to estimate both the Moho depth and MDC based on least-squares adjustment by elements. Chapter 5 concludes the thesis and outlines topics for future research.

### *1.4.3 Contents of Part two*

The thesis is based on 8 papers, which have already been published or submitted in international scientific journals. The publications will be referred to as Papers A-H as follows:

**PAPER A:**

Abrehdary, M., Sjöberg, L.E., and Bagherbandi, M. (2015). Modelling Moho depth in ocean areas based on satellite altimetry using Vening Meinesz–Moritz' method, (Published in Journal of Acta Geodaetica et Geophysica, 1-13).

**PAPER B:**

Abrehdary, M., Sjöberg, L.E., and Bagherbandi, M. (2015). Combined Moho parameters determination using CRUST1.0 and Vening Meinesz-Moritz Model, (Published in Journal of Earth Science, 26(4), 607-616).

**PAPER C:**

Abrehdary, M., Sjöberg, L.E., and Bagherbandi, M. (2015). The spherical terrain correction and its effect on the gravimetric-isostatic Moho determination, (Published in Geophysical Journal International, 204(1), 262-273).

**PAPER D:**

Abrehdary, M., Sjöberg, L.E., Bagherbandi, M., and Sampietro D. (2015) Modelling Moho parameters and their uncertainties from the combination of the seismic and satellite gravity data, (Submitted to Journal of Geodesy).

**PAPER E:**

Bagherbandi, M., Sjöberg, L.E., Tenzer, R., and Abrehdary, M. (2015). A new Fennoscandian crustal thickness model based on CRUST1.0 and a gravimetric–isostatic approach, (Published in Journal of Earth-Science Reviews, 145, 132-145).

**PAPER F:**

Bagherbandi, M., Tenzer, R., Sjöberg, L.E., and Abrehdary, M. (2015). On the residual isostatic topography effect in the gravimetric Moho determination, (Published in Journal of Geodynamics, 83, 28-36).

**PAPER G:**

Bagherbandi, M., Sjöberg, L.E., Bai, Y., Tenzer, R., Abrehdary, M. Miranda, S., and Sanchez, J.M. (2016). Effect of the lithospheric thermal state on the Moho geometry, (Submitted to Journal of South American Earth Science).

**PAPER H:**

Sjöberg, L. E., Abrehdary, M., and Bagherbandi, M. (2014). The observed geoid height versus Airy's and Pratt's isostatic models using matched asymptotic expansions, (Published in Journal of Acta Geodaetica et Geophysica, 49(4), 473-490).

# Chapter 2

# 2. Moho parameter determination based on gravimetric and seismic methods

There are two main methods for determining the depth of the Moho interface: gravimetric and seismic methods. In case of the gravimetric method of Moho determination, gravity data are employed under a certain isostatic hypothesis, which is based on isostatic equilibrium of the crust on the dense underlying mantle, whereas in the seismic method, Moho is identified as a surface where the velocity of the seismic wave changes (see Papers B, D and E).

The four most well-known isostatic models of estimating the Moho depth from gravity data can be listed as the Airy/Heiskanen (A/H), the Pratt/Hayford (P/H), the Vening Meinesz (VM), i.e. classical isostatic models, and the Vening Meinesz-Moritz (VMM) model. These models are described in the following.

## 2.1 The classical isostatic models

### *2.1.1 The Airy/Heiskanen model*

In 1855 G. B. Airy introduced an isostatic model that was later developed for geodetic purposes by W. A. Heiskanen. According to the Airy/Heiskanen theory the densities of the Earth's crust ( $\rho_0$ ) and mantle ( $\rho_1$ ) are assumed to be constant (usually, $\rho_0 = 2.67$ g/cm$^3$ and $\rho_1 = 3.27$ g/cm$^3$). The topographical masses of height *h* over the geoid are compensated in such a way that, the crustal root of density $\rho_0 < \rho_1$ penetrates down into the mantle at a depth *t* under a chosen compensation surface (see Heiskanen and Moritz, 1967, Section 3.4).

The isostatic mass compensation leads to the following equation:

$$\rho_0 h = (\rho_1 - \rho_0) t \tag{2.1}$$

from which *t* can be obtained accordingly.

For the oceans, it is similarly assumed that the crust has anti-roots with height $t'$. For water density $\rho_w \left(=1.03\ \text{g/cm}^3\right)$ and depth $h'$, the following equation holds:

$$t'\left(\rho_1 - \rho_0\right) = h'\left(\rho_0 - \rho_w\right) \tag{2.2}$$

Using known densities and formulas given above, the roots and anti-roots can be easily found to be proportional to the height of topography and the depth of the ocean, respectively,

$$t = 4.45\,h \quad \text{and} \quad t' = 2.73\,h' \tag{2.3}$$

The normal thickness of the Earth's crust is denoted by *T*; values of around

$$T_0 = 30\ \text{km} \tag{2.4}$$

are assumed. The crustal thickness under mountains is then

$$T_0 + h + t \tag{2.5}$$

and under the oceans it is

$$T_0 - h' - t' \tag{2.6}$$

It should be mentioned that the defined roots and anti-roots of the crustal thickness can be also obtained in a spherical approximation (e.g. Rummel et al. 1988).

### *2.1.2 The Pratt-Hayford model*

In 1855 J. H. Pratt proposed his model that was later put into a mathematical form by J. F. Hayford for geodetic applications. According to the Pratt/Hayford theory the mass density under mountains is assumed to be smaller than that under the oceans (see Heiskanen and Moritz, 1967, Section 3.4). The isostatic equilibrium is thus maintained by the following equation:

$$\left(D + h\right)\rho = D\rho_0 \tag{2.7a}$$

or

$$\rho_m - \rho_c = \frac{h}{D+h}\rho_c \tag{2.7b}$$

where $\rho_0 \left(= 2.67 \text{ g/cm}^3\right)$ and $\rho$ are the densities for $h = 0$ and $h > 0,$ respectively, and $D$ is the compensation depth (usually = 100 km). For the oceans, the compensating formulas become

$$\left(D - h'\right)\rho + h'\rho_w = D\rho_0 \tag{2.8a}$$

or

$$\rho - \rho_0 = \frac{h'}{D-h}\left(\rho_0 - \rho_w\right) \tag{2.8b}$$

*2.1.3 The Vening Meinesz regional model*

Both the A/H and P/H isostatic models are simplified to such an extent that the isostatic compensation is strictly local, which is not the case in reality. This is because '*'this presupposes free vertical mobility of the masses to a degree that is obviously unrealistic in this strict form''* (Heiskanen and Moritz 1967, Section 3.4). For this reason, F. A. Vening Meinesz (1931) modified the A/H theory and introduced a regional instead of local isostatic compensation based on flat Earth approximation. In Vening Meinesz' modification of A/H isostatic theory, the Earth's crust is regarded as a homogenous elastic plate, which is floating on a viscous mantle.

## 2.2 The Vening Meinesz-Moritz model

Typically, the classical isostatic models assume a uniform crustal density, without regarding the crustal density heterogeneities. This assumption propagates large errors into the Moho geometry estimated by gravity data, because the actual topography is not fully isostatically compensated. Furthermore, the sub-crustal density structures and additional geodynamic processes contribute to the overall isostatic balance (see Paper F). However, the VM model agrees better with reality than the first two classical isostatic models (i.e. A/H and P/H models), as it states that the isostatic compensation is regional rather

than local. Moritz (1990) improved the VM hypothesis to the global case, while regarding a spherical approximation of the Earth's surface. Sjöberg (2009) illustrated a new solution for the Moritz theory, named the Vening Meinesz-Moritz (VMM), and it is the main purpose of this chapter to estimate the Moho parameters based on this hypothesis.

### *2.2.1 Main concept of the VMM hypothesis*

The VMM isostatic problem is based on the condition that the isostatic gravity anomaly ($\Delta g_I$) vanishes. This states that the isostatic compensating attraction ($A_C$) fully compensates the Bouguer gravity anomaly ($\Delta g_B$) at observation point $P$ on the geoid surface (Sjöberg, 2009):

$$\Delta g_I(P) = \Delta g_B(P) + A_C(P) = 0, \tag{2.9a}$$

The defined Bouguer gravity anomaly is given by:

$$\Delta g_B(P) = \Delta g(P) - A^T(P) \tag{2.9b}$$

where $\Delta g$ is the (surface) gravity anomaly and $-A^T$ is the direct topographic effect on gravity (DITE) (see Sjöberg, 2013).

It should however, be pointed out that Eq. (2.9a) suffers from some problems due to the density variation within the crust (as crust has different layers) and the disturbing gravity signals from masses below the crust (i.e. non-isostatic effects) (Bagherbandi and Sjöberg, 2012; Bagherbandi et al. 2013). This is because the gravity data are generated by various sources, while the variable Moho topography is only one of them. Hence we have to remove these effects and the signal from density variations within the crust from Eq. (2.9a). The methodology used for correcting the gravity signal for such anomalies/disturbances is addressed in Chapter 3.

Another problem is that the Bouguer gravity anomaly used in Eq. (2.9a) still does not remove all topographic effects (Sjöberg, 2013; Sjöberg et al. 2015), but it needs also a reduction for the secondary indirect topographic effect (SITE).

*2.2.2 New definitions of Bouguer and isostatic gravity anomalies*

Recently Sjöberg (2013) and Sjöberg et al. (2015) have argued that the topographic reduction of the Bouguer anomaly is incomplete without applying the so-called secondary indirect topographic effect (SITE) or the indirect effect on the gravity anomaly, which leads to the no-topography gravity anomaly. This is because the gravity anomaly is related with the disturbing gravity potential ($T$) by the fundamental equation of physical geodesy in spherical approximation (Heiskanen and Moritz 1967, p. 29) as follows:

$$\Delta g = \frac{\partial T}{\partial r} - 2\frac{T}{r} = \delta g - 2\frac{T}{r}, \tag{2.10}$$

where $r$ is the geocentric radius (of the observation point). Accordingly, as $T = T^{NT} + V^T$, where $T^{NT}$ is the disturbing potential with the topographic signal $V^T$ removed, the relations between the DITEs are defined as follows (Sjöberg et al. 2015):

$$\Delta g^T = -A^T + 2\frac{V^T}{r}, \tag{2.11}$$

i.e. the DITE of the gravity anomaly ($\Delta g^T$) differs from that of the gravity disturbance ($-A^T$) by the term $2V^T/r$, which is the SITE. In other words, the Bouguer gravity anomaly, as defined by Eq. (2.9b), contains a remaining topographic contribution that is only removed after applying the SITE, while the no-topography gravity anomaly:

$$\Delta g^{NT} = \Delta g + \Delta g^T \tag{2.12}$$

is consistent with the Bouguer gravity disturbance with no remnant signal from the topography.

In a similar way, the traditional isostatic gravity anomaly, as above, does not fully compensate for the topographic attraction, but it also needs to be corrected in accordance with Eq. (2.12) to become the rigorous isostatic gravity anomaly (Sjöberg, 2013):

$$\Delta g_I^{new} = \Delta g^{NT} + A_C - 2\frac{V_C}{r} = \Delta g_I + 2\frac{V^T - V_C}{r}, \tag{2.13}$$

where the term $-2V_C/r$ is a remnant isostatic compensation, ''the secondary indirect isostatic effect'' (SIIE). Only by adding this term the isostatic gravity anomaly becomes consistent with the isostatic gravity disturbance:

$$\delta g_I(P) = \delta g_B(P) + A_C(P) = 0, \tag{2.14}$$

Below we focus on using only the gravity disturbance.

*2.2.3 The VMM solution by the refined Bouguer gravity disturbance*

Based on Sjöberg (2009), the isostatic compensation attraction can be divided into two terms:

$$A_C(P) = A_{C0}(P) + dA_C(P) \tag{2.15}$$

where $A_{C0}$ and $dA_C$ are the mean and the residual compensation attraction, respectively, and they can also be written as:

$$A_C(P) = k\left[\iint_{\sigma}\int_{R}^{R-T_0}\frac{r^2(r-r_P t)}{l_P^3}drd\sigma + \iint_{\sigma}\int_{R-T}^{R}\frac{r^2(r-r_P t)}{l_P^3}drd\sigma\right], \tag{2.16}$$

where $k = G\Delta\rho$, $G$ is the Newtonian gravitational constant, $\Delta\rho$ is the MDC, i.e. density contrast between the lower crust and uppermost mantle, $T_0$ is the normal (or mean) Moho depth, $\sigma$ is the unit sphere, $r_P$ and $r$ are the geocentric distances to the computation point and integration point, respectively, $l_P = \sqrt{r_P^2 + r - 2rr_P t}$, and $t = \cos\psi$, where $\psi$ is the geocentric angle between the computation and integration points. By inserting Eqs. (2.16) and (2.15) into Eq. (2.14), one obtains:

$$dA_C(P) = G\Delta\rho\iint_{\sigma}\int_{R-T}^{R}\frac{r^2(r-r_P t)}{l_P^3}drd\sigma = -\left[\delta g_B + A_{C0}\right] = -f(P) \tag{2.17}$$

According to Sjöberg (2009) and (2013), the last equation can be formulated and simplified in the following form:

$$-GR\Delta\rho\iint_{\sigma} K(\psi,s)\,d\sigma = f(P), \tag{2.18}$$

where $f(P)$ is given in Eq. (2.20) below, $R$ is the radius of the mean Earth sphere, $K$ is the integral kernel function of the spherical distance $\psi$ and the parameter $s(=1-T/R)$ ($s$ being a simple function of the Moho depth $T$, which is the unknown of the integral equation). The spectral representation of $K$ is given by:

$$K(\psi,s) = \sum_{n=0}^{\infty} \frac{n+1}{n+3}\left(1-s^{n+3}\right)P_n(\cos\psi), \tag{2.19}$$

where $P_n(\cos\psi)$ is the Legendre's polynomial of degree $n$.

The integral in Eq. (2.18) relates the variable Moho depth with the given values of the isostatic gravity disturbance. As for the isostatic gravity disturbance $\delta g_I$, the functional $f$ on the right-hand side of Eq. (2.17) is defined as follows:

$$f(P) = \delta g_B(P) + A_{C0}(P), \tag{2.20}$$

where $A_{C_0}(P)$ is the nominal compensation attraction, which is approximately given by:

$$A_{C_0}(P) \approx -4\pi k T_0 \tag{2.21}$$

*2.2.3.1 The VMM Moho depth*

The expression given in Eq. (2.18) is a non-linear Fredholm integral equation of the first kind for the unknown Moho depth. Its solution was presented under a second-order approximation by Sjöberg (2009) as:

$$T(P) = T_1(P) + \frac{T_1^2(P)}{R} - \frac{1}{32\pi R}\iint_{\sigma} \frac{T_1^2(Q)-T_1^2(P)}{\sin^3(\psi/2)}\,d\sigma_Q \tag{2.22}$$

where $T_1$ is the first-order approximation, defined by the spectral form:

$$T_1(P) = \sum_{n=0}^{\infty}\left(2 - \frac{1}{n+1}\right)\sum_{m=-n}^{n} f_{nm} Y_{nm}(P), \tag{2.23}$$

where $f_{nm}$ is the spherical harmonic coefficient of the isostatic gravity disturbance $f(P)$, and $Y_{nm}$ is the fully-normalized spherical harmonic of degree *n* and order *m*.

*2.2.3.2 The VMM Moho Density Contrast*

For obtaining MDC using the VMM method, Eq. (2.18) is rewritten, where MDC is not considered constant, as follows:

$$R\iint_{\sigma} \Delta\rho K(\psi, s)\, d\sigma = b(P), \tag{2.24a}$$

where

$$b(P) = -\left[\delta g_B + A_{C0}\right]/G \tag{2.24b}$$

and its series of spherical harmonic is given by:

$$b(P) = \sum_{n=0}^{\infty}\sum_{m=-n}^{n} b_{nm} Y_{nm}(P) \tag{2.24c}$$

In order to formulate the linearized observation equations for the product $T\Delta\rho$, the integral term on the left-hand side of Eq. (2.24a) can be expanded into a Taylor series to second order. By the substitution of the first two terms of the binomial series for $s^{n+3}$ from Eq. (2.19) to Eq. (2.24a) one can obtain (Sjöberg and Bagherbandi, 2011):

$$\begin{aligned} &R\iint_{\sigma} \Delta\rho K(\psi, s)\, d\sigma \\ &\approx 4\pi\sum_{n=0}^{\infty}\sum_{m=-n}^{n}\frac{n+1}{2n+1}\left[(\Delta\rho T)_{nm} - \frac{n+2}{2R}\left(\Delta\rho T^2\right)_{nm}\right] Y_{nm}(P), \end{aligned} \tag{2.25}$$

and from Eqs. (2.24a) and (2.24c), one can obtain the following solution for the product $T\Delta\rho$:

$$T\Delta\rho(P) \approx \sum_{n=0}^{\infty}\sum_{m=-n}^{n}\left[\frac{2n+1}{4\pi(n+1)}b_{nm} - \frac{n+2}{2}\left(\Delta\rho T^2\right)_{nm}\right]Y_{nm}(P), \quad (2.26)$$

Approximating $\left(\Delta\rho T^2\right)_{nm}$ by $T_0\left(\Delta\rho T\right)_{nm}$, the solution for $\Delta\rho$ becomes:

$$\begin{aligned}\Delta\rho(P) &\approx \frac{b(P)}{2\pi T(P)} \\ &- \frac{1}{4\pi T(P)}\sum_{n=0}^{\infty}\sum_{m=-n}^{n}\left[\frac{1}{n+1} - \frac{T_0/R}{2/(n+2) - T_0/R}\right]b_{nm}Y_{nm}(P),\end{aligned} \quad (2.27)$$

It states that if $T$ is known, the varying MDC can be estimated from the spectrum of $b$.

## 2.3 Seismic methods

### *2.3.1 Principle of the Methods*

The seismic methods are most effective for investigating the structure of the Earth's interior. They utilize different types of seismic waves like body waves (i.e. P-waves or compressional waves and S-waves or shear waves) and surface waves. The velocity of seismic waves is a key parameter in these methods. The propagation velocity of the seismic waves depends on the elastic properties and density of the medium. P-waves have a higher velocity than S-waves and they travel through any type of material, including fluid, while S-waves cannot travel in fluids, as fluids do not support shear stress (Schuck and Lange, 2007).

The seismic waves are usually generated by a hit (e.g. earthquake, explosion, volcano and or other natural sources) on the Earth's surface, and they travel within the subsurface. During their travelling through the subsurface seismic waves are reflected and refracted when elastic contrasts arise at boundaries between layers and rock masses of different rock properties (seismic velocities and/or bulk densities) or at man-made obstacles. By recording of seismic waves returning from

the subsurface to the surface, one can partially make conclusions on structures and lithological composition of the subsurface. By measuring the travel times of seismic waves and determining their material specific velocities, a geological model of the subsurface can be created (Schuck and Lange, 2007).

Since the 1920's, the seismic reflection and refraction waves have widely been used to study the structure of the Earth's interior, and man-made vibrations are often generated to investigate shallow, subsurface structures.

Accordingly, a useful explanation for the Moho interface is defined as that level in the Earth, where the velocity of body waves changes. Generally, in the Earth's lower crust the velocity of the P-waves and S-waves are approximately 7 and 4 km/s, while they abruptly increase to 8 and 4.6 km/s in the uppermost mantle. Thus, the P-waves and S-waves velocity contrast at the Moho discontinuity are about 1 and 0.5 km/s, respectively. This indicates a substantial change in the elastic parameters, resulting from a substantial change in the rock types in the crust and uppermost mantle (Grad and Tiira, 2012).

However, due to the limited coverage of seismic observations, their application for the recovery of the Moho interface is not merely offered, highlighting the need for using gravimetric data, jointly with other geophysical data.

## 2.4 The global Earth crustal model

Recently, several global models of the Earth's crust by means of seismic and gravimetric observations and also combination of them have been published. A summary of these models is described in the following.

### *2.4.1 The gravimetric models*

#### *2.4.1.1 DMM2.0*

The DMM2.0 model (Hamayun, 2014) is derived through the gravity disturbance together with two seismic models; CRUST1.0 (Laske et

al. 2013) and MDN07 (Meier et al. 2007). The resolution of the model is 2°×2°. The gravity disturbances are represented in terms of spherical harmonics coefficients. In order to remove the nuisance signal in the observed gravity disturbances, stripping corrections due to topography, bathymetry, ice, sediments, and other crust heterogeneities are applied.

*2.4.1.2 GEMMA1.0*

The GEMMA1.0 model (Reguzzoni and Sampietro, 2015) is an Earth crustal model based on GOCE satellite data and some prior seismic information. The model has a resolution of 0.5°×0.5° and it is composed of seven layers describing geometry and density of oceans, ice sheets, upper, medium and lower sediments, crystalline crust and upper mantle.

*2.4.2. The seismological models*

*2.4.2.1 CRUST1.0*

The CRUST1.0 model (Laske et al. 2013) is based on a new database of crustal thickness data from active source seismic studies as well as from receiver function studies. The new model is specified on a 1°×1° grid and incorporates 35 key crustal types that include the thickness, density and velocity of P-waves ($V_P$) and S-waves ($V_S$) for eight layers (ice, water, upper, middle, and lower sediments, upper, middle, and lower crust). The $V_P$ values are based on field measurements, whereas $V_S$ and density are calculated by using empirical $V_P$-$V_S$ and $V_P$-density relationships, respectively. For regions lacking field measurements, such as large parts of Africa, South America, Antarctica and Greenland, the seismic velocity structure of the crust is extrapolated from the average crustal structure for regions with similar crustal age and tectonic setting. The topography, bathymetry and ice cover are taken from ETOPO1 topographic/bathymetric model (Amante and Eakins, 2009). The sediment cover is based on the sediment model by Laske and Masters (1997), with some near-coastal updates.

*2.4.2.2 MDN07*

The MDN07 model (Meier et al. 2007) is derived from phase and group velocities of Rayleigh and Love waves, delivered with its corresponding uncertainties. The model has a formal resolution of 2°×2° but it is actually limited by the lateral resolution of the input phase and group velocity maps ranging between 500 and 1000 km. It has been computed using a neural network approach, which allows modeling the posterior Moho depth probability distribution. The whole procedure involves no linearization and the final solution is totally independent from the CRUST1.0 model (see Sampietro et al. 2013; Paper D).

*2.4.3 Combining the gravimetric and seismological models*

*2.4.3.1 KTH11C*

The KTH11C model (Sjöberg and Bagherbandi, 2011) is produced based on a preliminary combined solution to Vening Meinesz-Moritz global inverse problem for the Moho density contrast as well as for the Moho depth with a resolution of 2°×2° by using the data files of EGM2008 global gravitational field, the DTM2006 solid Earth topographic model and CRUST2.0 crustal model in a least squares procedure.

*2.4.3.2 GEMMA2012C*

The GEMMA2012C model (Reguzzoni et al. 2013) is partly derived in a similar way to the KTH11C model. In details, the model is generated by combining the seismic global model CRUST2.0 with gravity observations from the GOCE satellite mission for recovering both the Moho density contrast and Moho depth with a resolution of 0.5°×0.5°.

## 2.5 Uncertainties in the Moho parameters

Quantitative error estimates of Moho depth and MDC are of great importance to any usage of crustal model. Nevertheless, the evaluation of uncertainties in the Moho depth and MDC are usually overlooked.

Therefore, we tried to present a reasonable method to estimate the uncertainty in those observations of the VMM and CRUST1.0 models.

*2.5.1 Uncertainties in the VMM model*

Typically the uncertainties in the VMM Moho depth could be attributed on one hand to stochastic errors in the global gravity and topographic models as well as ice and sediment datasets ($\sigma_T^2$), and on the other hand to systematic biases due to unmodeled mantle (and crustal) density structures and geophysical processes. These biases propagate to the Moho geometry and causes disagreements between the gravimetric isostatic and seismic Moho models. The mean-square error (*MSE*) of the modeled Moho depth can be estimated as (see Bagherbandi et al. 2014):

$$MSE(T) = \sigma_T^2(P) + bias^2(T), \tag{2.28}$$

where the bias can be expressed:

$$bias(T) = \frac{1}{4\pi G\Delta\rho}\sum_{n=0}^{n_{\max}}\left(2-\frac{1}{n+1}\right)\sum_{m=-n}^{n} Y_{nm}(P)c_{nm}^{g^{NI}}. \tag{2.29}$$

Here $g^{NI}$ is the non-isostatic effect on gravity with its spherical harmonic coefficients $c_{nm}^{g^{NI}}$ as:

$$c_{nm}^{g^{NI}} = \frac{1}{4\pi}\iint_{\sigma} g^{NI}Y_{nm}(P)\,d\sigma, \tag{2.30}$$

Moreover, the variance of the MDC is estimated by (see Sjöberg and Bagherbandi, 2011):

$$\sigma_{\Delta\rho}^2 = \frac{\sigma_{T\Delta\rho}^2}{T_0^2} + \frac{\sigma_T^2(T\Delta\rho)^2}{T_0^4} \tag{2.31}$$

and the variance of $T\Delta\rho$ can also be approximated by the following formula (see Sjöberg and Bagherbandi, 2011):

$$\sigma^2_{T\Delta\rho} \approx \left(\frac{\gamma}{4\pi G}\right)^2 \sum_{n,m} N^2_{nm}\sigma^2_{nm} + 2\left(\frac{\gamma}{4\pi G}\right)^2 \sum_{n,m}\sum_{k,l\neq n,m} N_{nm}N_{kl}\sigma_{nmkl}, \quad (2.32)$$

where $\gamma$ is normal gravity, $N_{nm} = (2n+1)(n-1)/(n+1)$, $\sigma^2_{nm}$, and $\sigma_{nmkl}$ are the potential coefficient error degree and order variances and covariances, respectively (e.g. Pavlis and Saleh, 2004).

### *2.5.2 Uncertainties in the seismic crustal model*

The accuracies of the produced Moho contour maps are heavily affected by the uncertainties in the published interpretations of crustal structures. The uncertainties in the seismic crustal models arise from several factors such as the survey method, the spatial resolution of the survey, (for example the spacing of the shot points and the recording stations), and the analytical techniques utilized to process the data (Christensen and Mooney, 1995; Chulick et al. 2013).

It is indeed difficult to estimate the uncertainties associated to seismic crustal models of Moho depth and MDC, as the qualities of these models are not specified, and they vary a lot from place to place due to the accuracy as well as the quantity of available seismic observations.

The uncertainties are different in various seismic methods and can be different even for the same methods in different experiments and areas. For example, the lowest uncertainties are expected to be about 5 % of Moho depth for new and good-quality seismic refraction profiles and to be about 6–8 % for older, reinterpreted and compiled profiles. The lowest uncertainties about 20 % are assigned to results derived by surface waves and gravity modeling. The largest uncertainties of the Moho depths are strongly attributed to inaccuracies of crustal models currently available (Grad and Tiira, 2012).

Čadek and Martinec (1991) estimated Moho depth uncertainties in their global Moho model of the order 20 % (5 km) for the oceanic crust and of the order 10 % (3 km) for the continental crust. The results of more recent seismic and gravity studies, however, demonstrated that these error estimates are too optimistic. Grad and

Tiira (2009), for example, revealed that the uncertainties in the estimated Moho depths based on the seismic data under the Europe regionally are about 10 km with the average error of more than 4 km.

Much larger Moho uncertainties are expected over large portions of the world where the seismic data are sparse.

Similarly the errors in the MDC propagate proportionally to the errors in the estimated Moho depths.

### 2.6. Numerical investigations

We utilize the VMM model together with CRUST1.0 model to estimate the Moho undulations; first for ocean areas, and second for both land and ocean areas. In this way, different heterogeneous data have been used, including the global Earth gravity field model (e.g. DNSC08GRA and EGM2008), the global topography model (e.g. DTM2006 and Earth2014), and the global seismic crustal model (e.g. CRUST1.0). In the global study the data were compiled in a set of 1°×1° blocks. In details 21815 blocks onshore and 42985 blocks offshore were considered. A comparison of the Moho results with some other global models is presented in Tables 2.1 and 2.2 and also in Figs. 2.1 to 2.3 (see Papers A and C).

**Table 2.1.** Statistics of the Bouguer gravity disturbance and Moho depth computed through satellite altimetry. STD is the standard deviation of the estimated quantities over the ocean blocks. RMS is the Root Mean Square. $\delta g_B^{Altimetry}$ and $T^{Altimery}$ are the Bouguer gravity disturbance and VMM Moho depth estimated by satellite altimetry. $T^{GEMMA1.0}$ and $T^{CRUST1.0}$ are the GEMMA1.0 and CRUST1.0 Moho depths (see Paper A).

| Unit | Quantities | Max. | Mean | Min. | STD | RMS |
|---|---|---|---|---|---|---|
| **mGal** | $\delta g_B^{Altimetry}$ | 767.04 | 474.58 | 85.67 | 112 | |
| **km** | $T^{Altimetry}$ | 43.18 | 14.73 | 1.14 | 5.52 | |
| | $T^{Altimetry-GEMMA1.0}$ | 31.98 | 0.41 | -20.42 | 3.02 | 3.05 |
| | $T^{Altimetry-CRUST1.0}$ | 19.17 | 0.49 | -8.92 | 2.20 | 2.25 |

Table 2.1 illustrates that the Bouguer gravity disturbance, generated through satellite altimetry observations, varies from 86 to 767 mGal with a global average of 474 mGal and standard deviation of 112 mGal in ocean areas. It also shows that the VMM Moho depth computed by satellite altimetry data ranges from 43 to 1 km, with a global average of 15 km. As can also be seen from the table, the VMM Moho depth is compared with those from the GEMMA1.0 and CRUST1.0 models. By simple comparison of the VMM Moho depth in this study and the GEMMA1.0 model, we found out that the differences vary from -20.4 to 31.9 km, with a global average of 0.41 km and a RMS fit of 3 km. A similar comparison with the seismic CRUST1.0 model yields -8.9 to 19.1 km, with a global average and RMS fit of 2.2 km and 2.2 km, respectively.

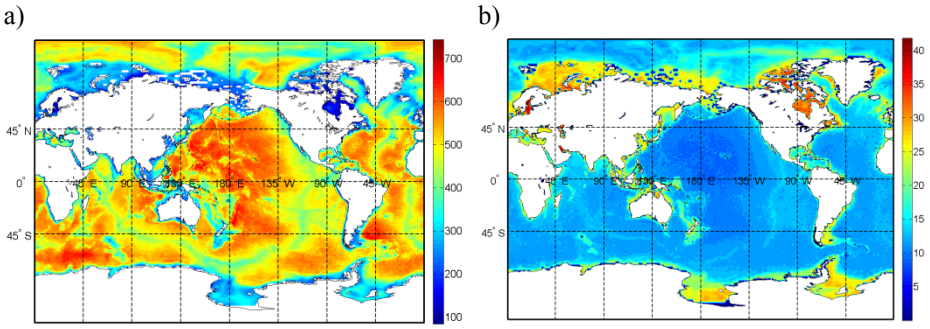


**Figure 2.1. (a)** The Bouguer gravity disturbance generated by satellite altimetry (in mGal), and **(b)** The Moho depth estimated via satellite altimetry (in km), (see Paper A)

As one can see in Fig. 2.1a, the large Bouguer gravity disturbances, generated by the DNSC08GRA global marine gravity field model, range to more than 700 mGal in ocean areas, whereas close to the continents they are generally small (see Paper A).

As shown in Fig. 2.1b, the Moho depths are generally less than 15 km in the ocean areas and along the oceanic ridges, but dominate to more than 30 km towards continental margins (see Paper A).

**Table 2.2.** Statistics of global estimates of the Bouguer gravity disturbance and Moho depth. STD is the standard deviation of the estimated quantities over the blocks. RMS is the Root Mean Square. $\delta g_{SSB}$ and $\delta g_{RSB}$ are the simple and refined spherical Bouguer gravity disturbance. $\delta g_{STC}$ is the calculated spherical terrain correction. $T^S$ and $T^R$ are the estimated VMM Moho depth based on the simple and refined Bouguer gravity disturbance. $T^{CRUST1.0}$ is the Moho depth derived by CRUST1.0 model. $T^S_{S.A}$, $T^R_{S.A}$, $T^S_{Fen}$, $T^R_{Fen}$, $T^{CRUST1.0}_{S.A}$ and $T^{CRUST1.0}_{Fen}$ are the estimated VMM Moho depths based on the simple and refined Bouguer gravity disturbance and those from CRUST1.0 in South America and Fennoscandia (see Paper C).

| Unit | Quantities | Max | Mean | Min | STD | RMS |
|---|---|---|---|---|---|---|
| mGal | $\delta g_{SSB}$ | 530.02 | 180.38 | -1326.5 | 244.8 | |
| | $\delta g_{STC}$ | 896.36 | 16.97 | -205.48 | 115.31 | |
| | $\delta g_{RSB}$ | 562.82 | 128.87 | -620.54 | 178.10 | |
| km | $T^S$ | 92.59 | 24.62 | 5.84 | 15.07 | |
| | $T^R$ | 64.53 | 23.09 | 5.84 | 12.57 | |
| | $T^R - T^{CRUST1.0}$ | 16.70 | 0.19 | -19.86 | 2.72 | 2.73 |
| | $T^S - T^{CRUST1.0}$ | 27.52 | 1.72 | -17 | 5.31 | 5.58 |
| | $T^S_{S.A} - T^{CRUST1.0}_{S.A}$ | 24.79 | 0.48 | -12.42 | 4.84 | 4.86 |
| | $T^S_{Fen} - T^{CRUST1.0}_{Fen}$ | 9.24 | -1.39 | -9.41 | 3.13 | 3.42 |
| | $T^R_{S.A} - T^{CRUST1.0}_{S.A}$ | 12.55 | -0.81 | -12.42 | 3.14 | 3.24 |
| | $T^R_{Fen} - T^{CRUST1.0}_{Fen}$ | 10.81 | -1.20 | -9.41 | 2.92 | 3.16 |

Table 2.2 demonstrates that the simple spherical Bouguer gravity disturbance corrected for density variation of bathymetry, ice and sediment varies between -1326.5 and 530 mGal with a global average and standard deviation of 180.4 mGal and 245 mGal. It also shows that the refined spherical Bouguer gravity disturbance ranges from -620.5 to 562.9 mGal, with a global average and standard deviation of 128.9 mGal and 178.1 mGal (see Paper C). As seen the Moho depths estimated from the simple spherical Bouguer gravity disturbance vary

from 6 to 93 km, with a global average and standard deviation of 25 km and 15 km. Similar to the Moho depths estimated via the simple spherical Bouguer gravity disturbance, the Moho depths estimated by the refined spherical Bouguer gravity disturbance vary from 6 to 65 km, with a global average and standard deviation of 23 km and 13 km, respectively. For evaluating the estimated results for the Moho depth (from the simple and refined Bouguer gravity disturbance), the CRUST1.0 seismic model is used. The RMS differences of the Moho depths estimated by the simple and refined spherical Bouguer gravity disturbances compared with that estimated by the seismic based CRUST1.0 model are 5.6 and 2.8 km, respectively.

Also in Table 2.2 one can see the considerable mean value differences from the estimated Moho depths (either simple or refined spherical Bouguer gravity disturbance) and the CRUST1.0 model, which are 1.8 and 0.2 km, respectively. These biases are caused by disagreements between the Moho depths estimated by the simple and refined cases on one hand and that by the CRUST1.0 model, and more so for the simple Bouguer case in comparison to the refined Bouguer case.

Table 2.2 also shows the Moho depths computed via VMM, before and after applying the terrain correction, and CRUST1.0 models in South America and Fennoscandia. These areas are most complicated areas in view of rough topography and post-glacial rebound. One can see that the RMS fits for the refined Bouguer gravity disturbances with CRUST1.0 are 3.3 and 3.2 km in South America and Fennoscandia, respectively. These values are about 33 % and 7.6 % smaller than the corresponding RMS fits of 4.9 and 3.4 km obtained from the simple Bouguer gravity disturbances.

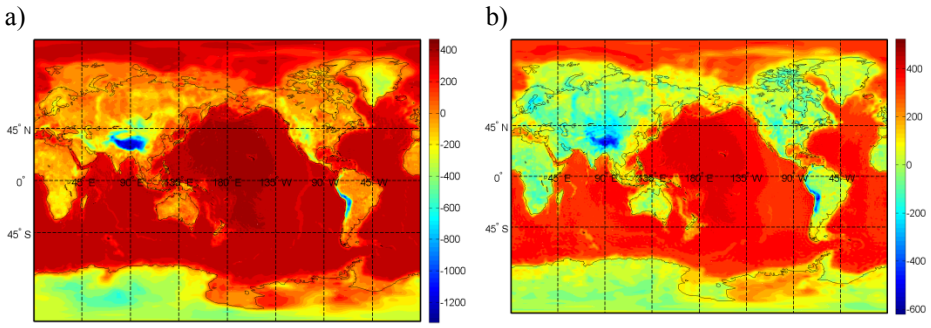


**Figure 2.2. (a)** The estimated simple spherical Bouguer gravity disturbance corrected for the bathymetry, ice, sediment and non-isostatic effects (unit mGal), and **(b)** The estimated refined spherical Bouguer gravity disturbance corrected for the bathymetry, ice, sediment and non-isostatic effects (unit mGal), (see Paper C).

Figure 2.2a depicts the simple spherical Bouguer gravity disturbances (i.e. only considering the gravitational of the spherical Bouguer shell without the terrain correction) corrected due to the ocean (bathymetry), ice, sediment variations and the NIEs, respectively.

As can be seen in Fig. 2.2b the refined spherical Bouguer gravity disturbances are generally negative, while oceanic areas are dominated by positive gravity values. The figure supports the theory that topographic masses are to much extent isostatically compensated.

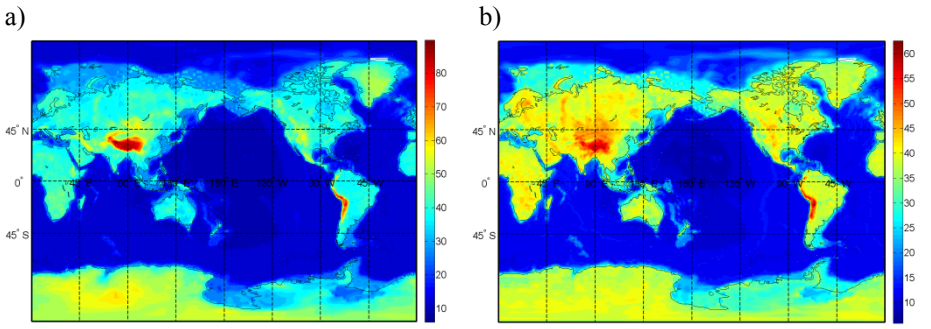


**Figure 2.3. (a)** The estimated VMM Moho depth based on the simple spherical Bouguer gravity disturbance, and **(b)** The estimated VMM Moho depth based on the refined spherical Bouguer gravity disturbance (in km) (see Paper C).

Figure 2.3a, showing the Moho depths estimated from the simple spherical Bouguer gravity disturbances, illustrates small Moho depths in the open ocean areas and along the oceanic ridges. As one would expect, in flat areas the simple Bouguer gravity disturbance can properly be used to remove most of the gravitational attraction of topographic masses, but in areas with rugged topography and near ocean coastlines, gravity disturbances are distorted by not correcting for the terrain features. Hence, in particular in these areas the simple Bouguer gravity disturbance must be improved by replacing it by the refined Bouguer disturbance, which means (at least theoretically) that the attraction of all the topographic mass has been removed.

In Fig. 2.3b the Moho depths computed via the refined spherical Bouguer gravity disturbances are shown. Similar to Fig. 2.3a, small Moho depths are generally seen in the ocean areas and along the oceanic ridges, increasing with topographic elevation in continental areas with maxima in Tibet and Andes. Comparing with Fig. 2.3a, one can see that the unrealistically extreme Moho depths of more than 90 km are now of order of 65 km, and the Moho depths in Greenland and Antarctica have also decreased all due to the applying the terrain correction. Also, the generally sharp changes of Moho depths along the continental margins in Fig. 2.3a are modified to smoother transition.

### *2.6.1 Uncertainties in the VMM and CRUST1.0 models*

Here a numerical study in order to investigate the uncertainties related to the VMM Moho depth and CRUST1.0 MDC models is performed (see Bagherbandi et al. 2014; Paper D). This is because, a proper understanding of these errors is necessary to secure the quality of the Moho results.

**Table 2.3.** Statistics of global estimates of the CRUST1.0 and VMM standard errors for 1°×1° block data. STD is the standard deviation. RMS is Root Mean Square. $S_{T^{VMM}}$ and $S_{\Delta\rho^{CRUST1.0}}$ are the standard error of the estimated Moho depth and CRUST1.0 MDC (see Paper D).

| Unit | Quantities | Max. | Mean | Min. | STD |
|---|---|---|---|---|---|
| **km** | $S_{T^{VMM}}$ | 0.90 | 0.72 | 0.66 | 0.03 |
| **kg/m$^3$** | $S_{\Delta\rho^{CRUST1.0}}$ | 166 | 73.76 | 39.99 | 34.60 |

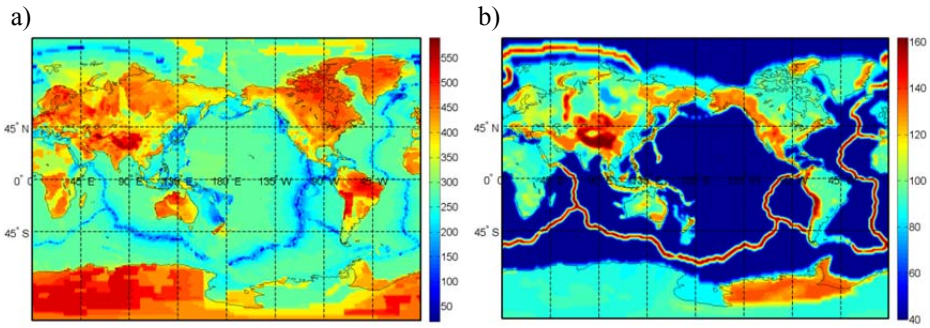


**Figure 2.4. (a)** The MDC derived by the CRUST1.0 model, and **(b)** standard errors of the MDC (in kg/m$^3$)

As one can see in Fig. 2.4a, the lowest MDCs are located in ocean areas, in particular along ocean ridges. As the oceanic ridges are special areas due to the presence of hot spots and light materials very close to the solid Earth topography due to the thinning of the oceanic crust, we get small MDCs in these regions. On the contrary, large MDCs are typically located in mountainous continental areas. The large MDCs in Antarctica are also notable.

Figure 2.4b depicts the CRUST1.0 MDC standard errors estimated in Paper D. From Fig. 2.4b one can see that for oceanic regions all standard errors are mostly less than 50 kg/m$^3$, whereas for continental regions, standard errors reach up to 120 kg/m$^3$.

The probable reasons for having the large errors in mountainous continental areas might be due to the uncertainties in the CRUST1.0, and for parts of Antarctica the uncertainty can be explained by the fact

that the density of ice topography was not properly distinguished from rock topography (see Paper D).

Furthermore, the ocean ridges have significant variations. As the ocean ridges have young lithospheric age (cf. Bagherbandi and Sjöberg, 2013; Paper B), the large errors in such regions are likely the lack in modelling the thermal expansion (the mantel convection).

## Chapter 3

# 3. Additive corrections to gravity disturbance

Nowadays, the Earth's gravity field has been recognized as an important source of information about the deep Earth's structure. These gravity data contain the short and long-wavelength features of the Earth structure, i.e. the signals from the topography and density heterogeneities related to bathymetry, ice, sediments and also from those in the mantle and core/mantle topography variations.

In other words, the long-wavelength contribution to the gravity field, say to degree and order 10, may be related to the mantle as well as core-mantle boundary topography (Sjöberg, 2009) and those between 11 to 35 degrees reflect the influence of Moho depth variations and lateral density anomalies of the crust (see Ellmann, 2004). And finally, the remaining short-wavelength contribution indicates smaller, near surface mass anomalies (see Corchete et al. 2010).

To isolate the gravity data caused only by the geometry of the Moho interface, all aforementioned signals contributors to the gravity data must be removed by applying the so-called stripping corrections and non-isostatic effects (Bagherbandi and Sjöberg, 2012; Bagherbandi et al. 2013; Tenzer et al. 2012 and 2015a).

### 3.1 Crust density variation corrections

In order to compute the refined Bouguer gravity disturbances, i.e. free-air gravity disturbances corrected for topography, bathymetry, ice thickness and sediment basins (i.e. stripping corrections), Tenzer et al. (2012) and (2015a) developed and applied a uniform mathematical formalism of computing the gravity corrections of the density variations within the Earth's crust by:

$$\delta g^{TBIS} = \delta g^{t} + \delta g^{b} + \delta g^{i} + \delta g^{s} \tag{3.1}$$

where $\delta g^t$ is the topographic gravity correction, and $\delta g^b$, $\delta g^i$ and $\delta g^s$ are the stripping gravity corrections due to the ocean (bathymetry), ice and sediment density variations, respectively.

Applying a spherical approximation of the Earth, the gravity corrections on the right-hand side of Eq. (3.1) are computed using the following expression:

$$\delta g^q(P) = \frac{GM}{R^2}\sum_{n=0}^{n_{max}}(n+1)\sum_{m=-n}^{n} c_{nm}^q Y_{nm}(P), \qquad (3.2)$$

where $GM = 3986005\times10^8\ \mathrm{m^3\,s^{-2}}$ is the geocentric gravitational constant. The (fully normalized) potential coefficients $c_{nm}^q$ of a particular volumetric mass density (or density contrast) layer $q$ (i.e., topography, bathymetry, glacial ice and sediments) are defined by:

$$c_{nm}^q = \frac{2}{(2n+1)}\frac{1}{\rho_e}\left[\frac{(\rho^q L_q)_{nm}}{R} + \frac{n+2}{2}\frac{(\rho^q L_q^2)_{nm}}{R^2} + \ldots\right] \qquad (3.3)$$

where $\rho^q$ is the Earth's mean mass density, and the coefficients ($\rho^q L_q^i$) are evaluated (from discrete data of density $\rho^q$ and thickness $L_q$) by applying a discretization to the following integral convolution

$$(\rho^q L_q)_{nm} = \frac{1}{4\pi}\iint_\sigma \rho^q L_q^j Y_{nm}(Q)\,d\sigma, \qquad j = 1, 2, \ldots, n \qquad (3.4)$$

### 3.2 Non-Isostatic Effects

It is important to remind that in general the crust is not in complete isostatic equilibrium and the observed gravity data are not only generated by the topographic/isostatic masses but also from those in the deep Earth interior, that leads to non-isostatic effects (NIEs) (see Bagherbandi and Sjöberg 2012 and 2013).

According to Sjöberg (2009) the major parts of the long-wavelengths of the geopotential are arisen by density variations in the Earth's

mantle and core/mantle topography variations. Such NIEs could be the contribution of different factors, such as crustal thickening/thinning, thermal expansion of mass of the mantle (Kaban et al. 2004), Glacial Isostatic Adjustment (GIA), plate flexure (Watts 2001, p. 114), and effect of other phenomena (Tenzer et al. 2009). This implies that this contribution to gravity will lead to systematic errors/NIEs of the computed Moho topography. Hence the NIEs should also be corrected on the isostatic gravity disturbance.

Assuming that the seismic Moho model CRUST1.0 is known and correct, the gravity effect of the NIEs can be determined by:

$$\delta g^{NIE} = \frac{GM}{R^2}\sum_{n=0}^{n_{max}}(n+1)\sum_{m=-n}^{n} c_{nm}^{NIE} Y_{nm}(P) \tag{3.5}$$

where

$$c_{nm}^{NIE} = c_{nm}^{\mathrm{CRUST1.0}} - c_{nm}^{VMM} \tag{3.6}$$

The spherical harmonic coefficients $c_{nm}^{j}$ ($j$ = VMM, CRUST1.0) in Eq. (3.6) are generated using the following expression

$$c_{nm}^{j} \approx \frac{3}{(2n+1)R\rho_e}\left[\left(\Delta\rho\left(T_j - T_0\right)\right)_{nm} + \frac{(n+2)\left(\Delta\rho(T_0^2 - T_j^2)\right)_{nm}}{2R^2}\right] \tag{3.7}$$

Here $\rho_e\left(\approx 5.5\ \mathrm{g/cm^3}\right)$ is the Earth's mean density, $\mathrm{R}\left(=6371\times10^3\ \mathrm{m}\right)$ is the Earth's mean radius (which approximates the geocentric radius of the geoid surface), $T_{VMM}$, $T_{\mathrm{CRUST1.0}}$ and $T_0$ are the VMM and CRUST1.0 Moho depths and its mean value (approximately 23 km based on CRUST1.0 model), respectively. $\Delta\rho$ is the constant MDC and the spherical harmonic coefficients $\left(\Delta\rho\left(T_j - T_0\right)\right)_{nm}$, $\left(\Delta\rho\left(T_j^2 - T_0^2\right)\right)_{nm}$ are defined for the following products of the MDC and depth: $\Delta\rho\left(T_j - T_0\right)$, $\Delta\rho\left(T_j^2 - T_0^2\right)$.

Taking into consideration the gravitational contribution of the crust density heterogeneous, the non-isostatic effects are applied to the isostasy gravity disturbance $\delta g_I$. The isostatic equilibrium equation in Eq. (2.9a) is then rewritten as:

$$\delta g_I(P) = \delta g_B^{TBISN}(P) + A_{C0}(P) = 0. \tag{3.8}$$

Here $\delta g_B^{TBISN}$ is the refined Bouguer gravity disturbance corrected for the gravitational contributions of topography and density variations of the oceans, ice, sediments and NIEs.

Combining Eqs. (3.1) and (3.8), the fundamental formula of solving the VMM problem in Eq. (2.19) becomes

$$-GR\Delta\rho \iint_\sigma K(\psi, s)\, d\sigma = \left[\delta g_B^{TBISN} + A_{C0}\right], \tag{3.9}$$

### 3.3. Numerical investigations

The gravity disturbances are corrected in two main ways namely for the gravitational contributions of mass density variation due in different layers of the Earth's crust such as ice and sediments, as well as for the gravity contribution from deeper masses below the crust (i.e. NIEs).

The statistics of the gravity corrections and respective corrected gravity disturbances are presented in Tables 3.1. The gravity corrections are computed using the recent seismic crustal thickness model CRUST1.0 with a resolution of 1°×1°.

**Table 3.1.** Statistics of global estimates of the gravity disturbances, stripping gravity corrections and NIEs. STD is the standard deviation of the estimated quantities over the blocks. $\delta g$ is the gravity disturbances computed by the GOCO03S coefficients (Mayer-Gürr et al. 2012). $\delta g^b$, $\delta g^i$, and $\delta g^s$ are the bathymetric, ice and sediment stripping gravity corrections derived from the CRUST1.0, respectively. $\delta g_{NIE}$ is the non-isostatic effects. $\delta g^{TBISN}$ is the refined Bouguer gravity disturbance after applying the topographic and stripping gravity corrections due to the ocean, ice and sediment density variations (see Paper C).

| Unit | Quantities | Max | Mean | Min | STD |
|---|---|---|---|---|---|
| mGal | $\delta g$ | 285.85 | -0.44 | -281.40 | 23.84 |
| | $\delta g^T$ | 255.13 | -71.06 | -647.61 | 105.98 |
| | $\delta g^B$ | 721.60 | 332.91 | 110.28 | 165.02 |
| | $\delta g^I$ | 325.78 | 21.84 | -2.61 | 56.57 |
| | $\delta g^S$ | 185.31 | 45.48 | -0.02 | 32.47 |
| | $\delta g_{NIE}$ | 248.70 | -134.65 | -497.98 | 69.98 |
| | $\delta g^{TBISN}$ | 562.82 | 128.87 | -620.54 | 178.10 |

Figure 3.1 depicts the Bouguer gravity disturbances corrected due to the ocean (bathymetry), ice, sediment variations and the NIEs, respectively. As one can see from Fig. 3.1, these features can drastically change the Bouguer gravity disturbances from the free-air disturbances over oceans due to the application of the bathymetric stripping gravity correction. They also change in central Greenland and Antarctica due to application of the ice density variation stripping gravity correction and change less remarkably due to applying the sediment density variation stripping gravity correction in polar areas (see Paper C).

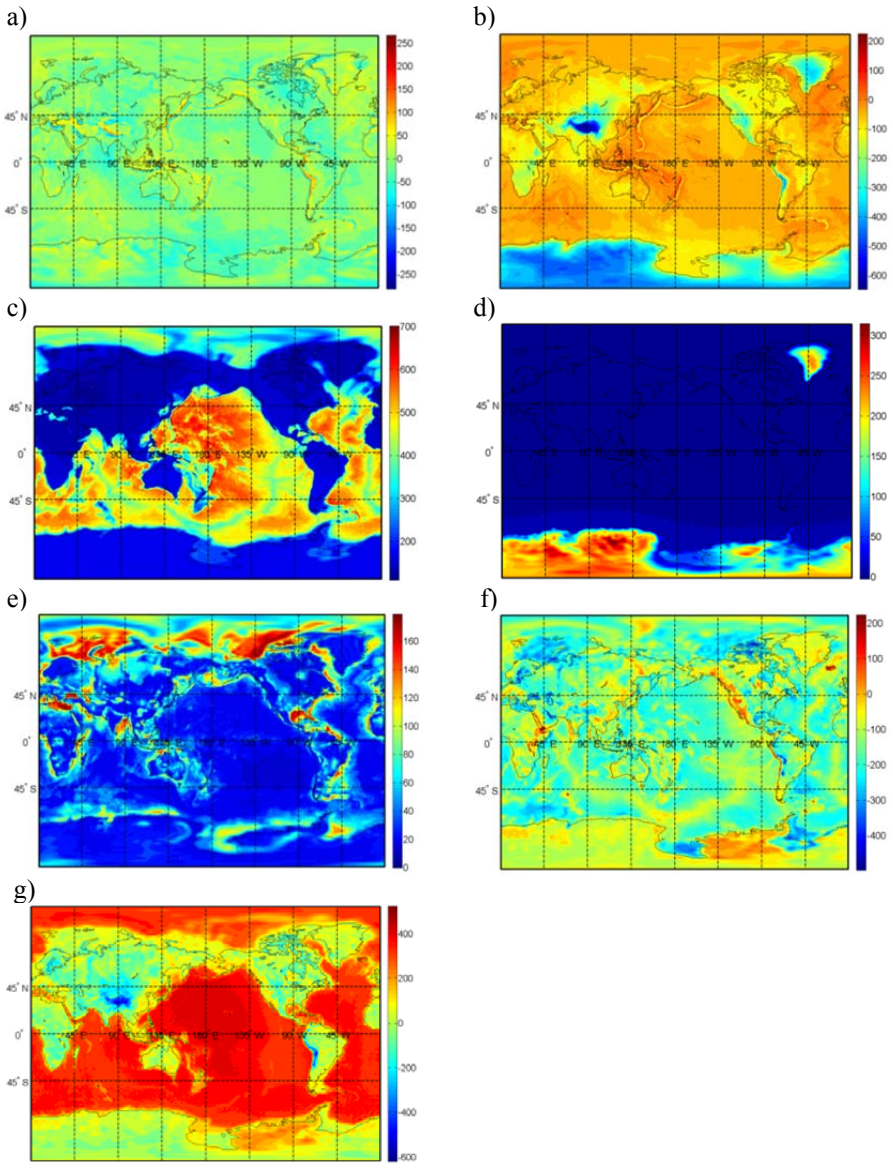


**Figure 3.1. (a)** The free-air gravity disturbance computed using the GOCO03S coefficients complete to degree 180 of spherical harmonics, **(b)** The topographic gravity correction, **(c)** The bathymetric stripping gravity correction, **(d)** The ice density variation stripping gravity correction, **(e)** The sediments density variation stripping gravity corrections, **(f)** non-isostatic effects and **(g)** refined Bouguer gravity disturbances after applying the topographic and stripping gravity corrections due to the ocean, ice, sediment density variations and non-isostatic effects (unit mGal)

## Chapter 4

# 4. The combined approach

Generally, the Moho interface is delineated accurately through seismic observations, but the limited coverage of such observations and economic considerations make gravimetric or combined gravimetric-seismic data a more realistic technique for imaging Moho models.

### 4.1 Combining the gravimetric and seismic models

Our main purpose in this chapter is simultaneously to estimate the Moho depth and MDC by combining gravimetric and seismic models. Our method is based on a linearized least-squares adjustment by elements. Basically $T\Delta\rho$, estimated by means of gravity observations, is combined with independent a priori estimates $T_0$ and $\Delta\rho_0$ of those parameters, with the goal of getting separate improved estimates of each parameter (see Sjöberg and Bagherbandi, 2011; Papers B, D, and E). To that end, we form the system of (linearized) observation equations as:

$$\mathbf{A}\,\mathbf{x} = \mathbf{L} - \boldsymbol{\varepsilon} \tag{4.1}$$

where

$$\mathbf{A} = \begin{bmatrix} \Delta\rho_0 & T_0 \\ 0 & 1 \\ 1 & 0 \end{bmatrix}, \qquad \mathbf{x} = \begin{bmatrix} \delta T \\ \delta\Delta\rho \end{bmatrix} \qquad \text{and} \qquad \mathbf{L} = \begin{bmatrix} l_1 - T_0\Delta\rho_0 \\ l_2 - \Delta\rho_0 \\ l_3 - T_0 \end{bmatrix}. \tag{4.2}$$

Here, the observation vector **L** in Eq. (4.2) is composed of three observations, namely $l_1 = T\,\Delta\rho$ (Eq. 2.26) and both $l_2 = \Delta\rho$ and $l_3 = T$ are derived by the values of the seismic crustal models, respectively, and $\delta T$ and $\delta\Delta\rho$ are the corrections to the priori estimates $T_0$ and $\Delta\rho_0$ of $T$ and $\Delta\rho$, and $\varepsilon_i$ are the observation errors.

The least squares solution of this system of equations becomes:

$$\hat{\mathbf{x}} = \left(\mathbf{A}^{\mathbf{T}}\mathbf{Q}^{-1}\mathbf{A}\right)^{-1}\mathbf{A}^{\mathbf{T}}\mathbf{Q}^{-1}\mathbf{L} \tag{4.3}$$

The covariance matrix $\mathbf{Q}_{\hat{\mathbf{x}}}$ of the estimated parameters is given by:

$$\mathbf{Q}_{\hat{\mathbf{x}}} = \sigma_0^2\left(\mathbf{A}^{\mathbf{T}}\mathbf{Q}^{-1}\mathbf{A}\right)^{-1} \tag{4.4}$$

Here $\mathbf{Q}$ is the covariance matrix of $\mathbf{L}$ and $\sigma_0^2$ is the variance of the unit weight which can be estimated by:

$$\sigma_0^2 = \mathbf{L}^{\mathbf{T}}\mathbf{Q}^{-1}(\mathbf{L} - \mathbf{A}\hat{\mathbf{x}}) \tag{4.5}$$

Finally, the least-squares solutions for both the Moho depth and MDC are given by:

$$\hat{T} = T_0 + \delta\hat{T} \tag{4.6}$$

and

$$\Delta\hat{\rho} = \Delta\rho_0 + \delta\Delta\hat{\rho} \tag{4.7}$$

where $\delta\hat{T}$ and $\delta\Delta\hat{\rho}$ are the estimated improvements to $T_0$ and $\Delta\rho_0$.

### 4.2. Numerical investigations

A combined solution for both the Moho depth and the MDC was given above. In the numerical solution, the priori estimates of Moho depth and MDC are needed, which are obtained from MDN07 (Meier et al. 2007) and CRUST1.0 models and $T\Delta\rho$ is estimated by Eq. (2.26) (see Papers B, D and E).

**Table 4.1.** Statistics of global estimates of the combined approach for 1°×1° block data. STD is the standard deviation. RMS is Root Mean Square. $\hat{T}$ is the estimated Moho depth from combined approach, $d\hat{T}$ is the estimated improvement to $T_0$, and $S_{\hat{T}}$ is the standard error of the estimated Moho depth. $\Delta\hat{\rho}$ is the estimated MDC from combined approach, $d\Delta\hat{\rho}$ is the estimated improvement to $\Delta\rho_0$, and $S_{\Delta\hat{\rho}}$ is the standard error of the estimated MDC. $T^{CRUST1.0}$ and $T^{KTH14C}$ are the Moho depths derived from CRUST1.0 and KTH14C models. $\Delta\rho^{KTH11C}$ and $\Delta\rho^{KTH14C}$ are the MDC derived by the KTH11C and KTH14C models (see Paper D).

| Unit | Quantities | Max. | Mean | Min. | STD | |
|---|---|---|---|---|---|---|
| km | $\hat{T}$ | 70.15 | 23.37 | 6.57 | 12.98 | |
| | $d\hat{T}$ | 18.98 | -2.71 | -38.70 | 5.27 | |
| | $S_{\hat{T}}$ | 8.20 | 1.27 | 0.00 | 0.91 | |
| | $\hat{T}-T^{KTH14C}$ | 21.68 | -0.45 | -35.28 | 4.34 | 4.36 |
| | $\hat{T}-T^{CRUST1.0}$ | 16.99 | 0.51 | -18.58 | 3.10 | 3.15 |
| kg/m$^3$ | $\Delta\hat{\rho}$ | 679.83 | 345.37 | 21 | 111.72 | |
| | $d\Delta\hat{\rho}$ | 471.43 | -15.06 | -604.70 | 114.72 | |
| | $S_{\Delta\hat{\rho}}$ | 132.87 | 20.26 | 0.07 | 14.70 | |
| | $\Delta\hat{\rho}-\Delta\rho^{KTH11C}$ | 269.15 | -75.21 | -492.33 | 93.37 | 119.9 |
| | $\Delta\hat{\rho}-\Delta\rho^{KTH14C}$ | 585.85 | 23.24 | -395.75 | 76.84 | 80.28 |

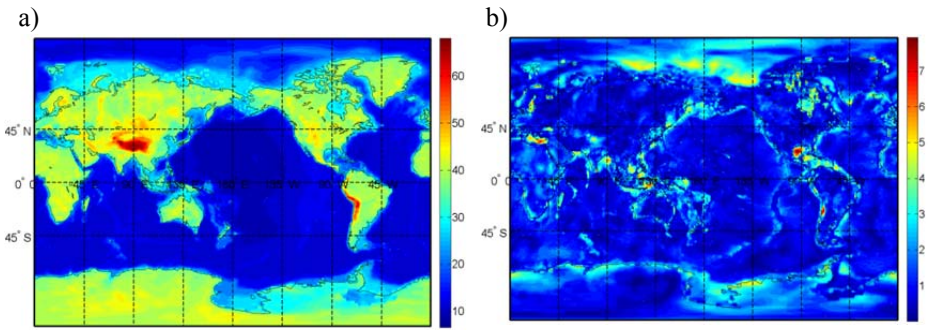


**Figure 4.1. (a)** The Moho depth estimated from combined approach, and **(b)** standard errors of the estimated Moho depth (unit km)

Figure 4.1a exhibits the Moho depth computed by the combined approach. As one would expected, the largest depths in the continental crust are seen in the mountainous regions Tibet and Andes, while smaller Moho depths are generally seen in the oceanic areas and in particular along the oceanic ridges. Note how well the estimated Moho depths follow the topography.

Figure 4.2b maps the estimated Moho depth standard errors. One can observe that the standard errors in oceanic regions are smaller than 3 km, whereas for continental regions the standard errors grow up to 7 km. Similar to Fig. 4.1b, notable errors are seen in the Gulf of Mexico, Chile, Eastern Mediterranean, Timor sea and parts of polar regions, which could be partly due to the failure of properly modelling the sediment thickness in the CRUST1.0 model, to the uncertainties in the MDN07 model, and also due to a mismodeling the density of ice topography from rock topography in polar regions.

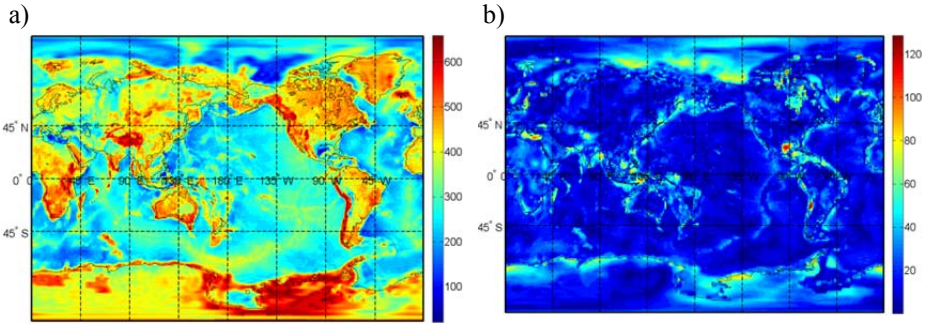


**Figure 4.2. (a)** The MDC estimated by combined approach, and **(b)** standard errors of the MDC (unit kg/m$^3$)

Since the MDC is highly dependent on the properties of the crust and upper mantle of the study area, it is partially difficult to provide a standard value for it. However, as can be seen from Fig. 4.2a, the largest MDCs are concentrated in mountainous continental areas, for example in the Tibet and Andes and parts of Antarctica, whereas smaller MDCs are seen in ocean areas.

Figure 4.2b maps the MDC standard errors estimated by the combined approach. From Fig. 4.2b one can see that for oceanic regions all

standard errors are mostly less than 50 kg/m$^3$, while for continental regions, standard errors reach up to 120 kg/m$^3$.

The probable reasons for having the large errors in the Gulf of Mexico, Eastern Mediterranean and Timor sea could be attributed to the lack in modelling of the sediment thickness in the CRUST1.0 (see Paper B). For Chile the error might be due to the uncertainties in the CRUST1.0, and for polar regions the uncertainty can be explained by the fact that the density of the ice topography was not properly distinguished from rock topography.

**Table 4.2.** Sources of regional Moho depth models used in this study

| Model ID | Resolution | Region | Survey type |
|---|---|---|---|
| SAM10 (Lloyd et al. 2010) | 2°×2° | South America | Receiver function |
| NAM02 (Chulick and Mooney, 2002) | 1°×1° | North America | Seismic refraction and other seismic data |
| AFR07 (Pasyanos and Nyblade, 2007) | 1°×1° | Africa | Fundamental-mode surface wave |
| EUP09 (Grad and Tiira, 2009) | 0.1°×0.1° | Europe | Body and surface waves, receiver function and other seismic data |
| ASA03 (Marone et al. 2003) | 2°×2° | Asia | Seismic refraction, reflection and receiver function |
| AUS11 (Kennett, 2011) | 0.5°×0.5° | Australia | Receiver function |
| ANT13 (Baranov and Morelli, 2013) | 1°×1° | Antarctica | Seismic refraction, reflection and tele seismic receiver function |

As can be seen in Table 4.2, in order to validate the quality of our estimated Moho depth, some regional models SAM10, NAM02, AFR07, EUP09, ASA03, AUS11 and ANT13 are used (see Paper D).

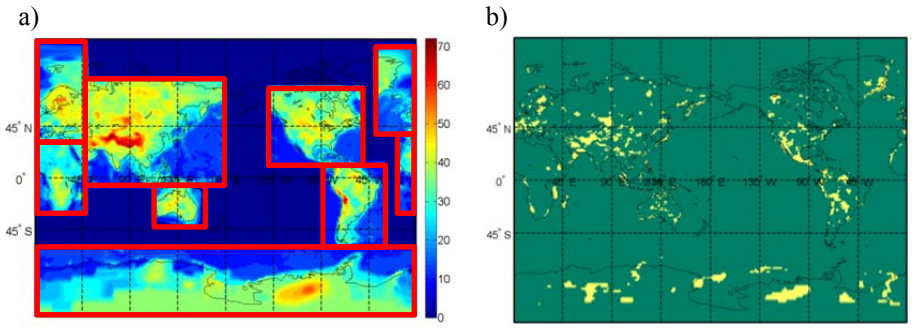


Figure **4.3. (a)** Regional map of seismic estimates of the Moho depth used in this study (in km), and **(b)** Coherence between combined approach and Moho depths from seismic regional models.

Figure 4.3a shows the regional Moho depths derived from seismic information in South and North America, Africa, Europe, Asia, Australia and Antarctica, respectively, and Fig. 4.3b depicts the coherence between combined approach and these Moho depths. The latter figure shows that Moho depths of the combined approach agree with the seismic estimates in 93 per cent of the locations, illustrating that there is a reasonably good agreement between the two sets. The main discrepancies are located in the areas of transition between continental and oceanic crust, which could be attributed to the different resolutions of each model and or to imperfect estimates in combined approach and seismic models. In Fig. 4.3a yellow areas indicate that the two models are not consistent, this of course can be do either to an error in terms of Moho depth or to a wrong estimate of the model accuracy (see Paper D).

# Chapter 5

# 5. Conclusions and Future Research

## 5.1 Conclusions

The study of the Moho discontinuity has become a crucial topic in inferring the dynamics of the Earth's interior for a long time. In general, the Moho can be studied with profitable results through seismic data. However due to the sparsity of seismic data in parts of the world, it has not been well determined. With the advent of satellite missions, it has been possible to recover the Moho parameters (i.e. Moho depth and Moho density contrast) via satellite gravity observations based on isostatic models.

So far, various isostatic models have been presented for recovering the Moho parameters (see Section 1.3), but it was not clarified which one is most appropriate to employ for geophysical and geodynamical purposes. The preliminary and simplest isostatic models proposed are the classical ones, with a local and regional compensation. However, those models cannot image realistically the actual Moho undulation. This is because they suppose a uniform crustal density, while disregarding the density irregularities distributed within the crust and sub-crust.

Understanding this important role of Moho recovery, its determination has been in the centre of the discussions by many geoscientists during the last decades. Therefore, we undertook the task of determination of Moho parameters and their uncertainties based on the VMM and the combined methods via gravimetric and seismic data over regional and global scales to a resolution of 1°×1°. First of all, this is because the VMM model (in contrast to the classical models) is based on a global isostatic compensation, which makes it more realistic than the classical ones. Moreover, the combined method (i.e. combination of the gravimetric and seismic data) can diminish substantially the seismic data gaps and provide a high resolution data coverage.

The main input data utilized for a Moho recovery in the thesis, either on the VMM or the combined methods, are the gravity anomaly/disturbance observations together with data from seismological models (e.g. CRUST1.0 and MDN07). The observed gravity data contains disturbing signals from the topography and density heterogeneities associated to bathymetry, ice, sediments and also from those in the mantle and core/mantle topography variations. Therefore, in order to isolate the gravity data caused only by the geometry of the Moho, aforementioned signal contributors to the gravity data are tried to be suppressed by applying the stripping gravity corrections and non-isostatic effects. The corrections are calculated using CRUST1.0.

To fulfil the goals of the thesis, we performed various studies as reported in the 8 papers of Part two, which are accepted or submitted in refereed journals. Based on the numerical investigations in these papers we found that:

The VMM approach in predicting Moho depth using a global marine gravity field model obtained by satellite altimetry data is applied successfully over the oceans, and the possible mean dynamic topography in the marine gravity model cannot substantially affect the Moho determination.

The utilization of the refined spherical Bouguer gravity disturbance in the VMM method for finding the Moho depth improved the RMS fits of our Moho results with the CRUST1.0 Moho model about 51 % compared to result obtained by using the simple spherical Bouguer gravity disturbance (i.e. only considering the gravitational of the spherical Bouguer shell without the terrain correction), implying that despite the fact that the lateral variation of the crustal depth is rather smooth, the terrain affects the Moho result most significantly in many areas.

The application of the lithospheric thermal-pressure correction (i.e. the contribution of the lithospheric thermal state) to the gravity data improved the disagreement between the VMM gravimetric Moho

solution to the CRUST1.0 seismic model about 40 % in South America, particularly over oceans and continental margins.

In an overall view, there is a relation between the degrees of isostatic compensation (i.e. complete and incomplete compensation) and geological structures in Fennoscandia, which can affect the Moho geometry. In details the geological features are related to different compensation-ratios, showing that a lower compensation-ratio denotes a stronger geological unit.

The isostatic gravity bias due to disagreement between the actual and isostatically compensated topographies corresponds to the Moho correction, so that applying this correction to the gravimetrically determined Moho depth significantly improves the RMS fit of our gravimetric result with some published global Moho models about 20 % and it also improves RMS fit about 46 % in some regions (e.g. Fennoscandia).

The combined approach is able to simultaneously estimate the Moho parameters (i.e. Moho depth and Moho density contrast) with corresponding uncertainties by combining gravimetric and seismic information based on a linearized least-squares adjustment model. The Moho parameters computed by the combined approach provide good fit to all other regional and global models in 90 per cent of the locations.

The geoid height can hardly be successfully modelled by the classical isostatic models due to the many other signals from various mass variations within the Earth that affects the geoid.

### 5.2 Future research

Some recommendations for future work can be considered as follows:

**1.** As can be seen in this thesis, the resolution of our Moho results depends on the CRUST1.0 model that is used. This is because in the method we use the global additive corrections are calculated using this model. It is therefore recommended to produce Moho models of

higher spatial resolution, once a global crustal model of higher resolution becomes available.

**2.** The combined approach used in this study faces a problem in some rift zones, most likely due to too rough a priori values in the least squares procedure after linearization of the original nonlinear equations. This problem is recommended to be considered in a forthcoming study.

**3.** Recently, a huge improvement has been observed in the accuracy and spatial resolution of global gravity field models, which are achieved by using the new data of the GOCE satellite mission. It is recommended to apply the improved gravity models for updating the Moho model.

**4.** The current study can further be extended in modeling other boundaries, for example, the core-mantle boundary (or Gutenberg discontinuity).

**5.** The classical isostatic models applied in this research estimate the geoid well over neither global nor regional scales. Therefore a study for a more reasonable isostatic model in predicting the geoid undulations (e.g. VMM model) is still open.

# Bibliography


Airy, G. B. (1855). On the computation of the effect of the attraction of mountain-masses, as disturbing the apparent astronomical latitude of stations in geodetic surveys. *Philosophical Transactions of the Royal Society of London*, 101-104.

Amante, C., and Eakins, B. W. (2009). ETOPO1 1 Arc-Minute global relief model: Procedures, data sources and analysis–NOAA technical memorandum NESDIS NGDC-24.

Anderson, D.L. (1989). *Theory of the Earth*. Blackwell Scientific Publications.

Bagherbandi, M., and Sjöberg, L. E. (2012). Non-isostatic effects on crustal thickness: a study using CRUST2. 0 in Fennoscandia. *Physics of the Earth and Planetary Interiors*, *200*, 37-44.

Bagherbandi, M., and Sjöberg, L. E. (2013). Improving gravimetric–isostatic models of crustal depth by correcting for non-isostatic effects and using CRUST2.0. *Earth-Science Reviews*, *117*, 29-39.

Bagherbandi, M., Tenzer, R., and Sjöberg, L. E. (2014). Moho depth uncertainties in the Vening-Meinesz Moritz inverse problem of isostasy.*Studia Geophysica et Geodaetica*, *58*(2), 227-248.

Bassin C., Laske G., Masters T.G. (2000). The current limits of resolution for surface wave tomography in North America, *Eos Trans. AGU*.

Čadek, O., and Martinec, Z. (1991). Spherical harmonic expansion of the Earth's crustal thickness up to degree and order 30. *Studia Geophysica et Geodaetica*, *35*(3), 151-165.

Christensen, N., and Mooney, W. (1995). Seismic velocity structure and composition of the continental crust: A global view. *Journal of Geophysical Research Atmospheres*, (100), 9761-9788.

Chulick, G. S., and Mooney, W. D. (2002). Seismic structure of the crust and uppermost mantle of North America and adjacent oceanic basins: a synthesis. *Bulletin of the Seismological Society of America*, *92*(6), 2478-2492.

Chulick, G. S., Detweiler, S., and Mooney, W. D. (2013). Seismic structure of the crust and uppermost mantle of South America and surrounding oceanic basins. *Journal of South American Earth Sciences*, *42*, 260-276.

Corchete, V., Chourak, M., and Khattach, D. (2010). A methodology for filtering and inversion of gravity data: an example of application to the determination of the Moho undulation in Morocco. *Engineering*, *2*(03), 149.

Ellmann, A. (2004). Effect of GRACE satellite mission to gravity field studies in Fennoscandia and the Baltic Sea region. *Proceedings of the Estonian Academy of Science, Geology, GRACE study*, *53*, 67-93.

Grad, M., and Tiira, T. (2009). The Moho depth map of the European Plate.*Geophysical Journal International*, *176*(1), 279-292.

Grad, M., and Tiira, T. (2012). Moho depth of the European Plate from teleseismic receiver functions. *Journal of seismology*, *16*(2), 95-105.

Hamayun, H. (2014). *Global Earth Structure Recovery from State-of-the-art Models of the Earth's Gravity Field and Additional Geophysical Information*(Doctoral dissertation, TU Delft, Delft University of Technology).

Hayford, J. F. (1909). *Geodesy: The Figure of the Earth and Isostasy from Measurements in the United States* (No. 82). US Government Printing Office.

Heiskanen, W. A., (1924). Untersuchungen ueber Schwerkraft und Isostasie. Finn. Geod. Inst. Publ. No. 4, Helsinki.

Heiskanen,W. A. (1938). New isostatic tables for the reduction of the gravity values calculated on the basis of Airy’s hypothesis. Isostat. Inst. of IAG Publ. No. 2. Finnish Geodetic Institution, Helsinki.

Heiskanen, W.A. and Moritz, H. (1967). Physical Geodesy. W.H. Freeman, New York.

Kaban, M. K., Schwintzer, P., and Reigber, C. (2004). A new isostatic model of the lithosphere and gravity field. *Journal of Geodesy*, *78*(6), 368-385.

Kearey, P., Brooks, M., and Hill, I. (2013). *An introduction to geophysical exploration*. John Wiley and Sons.

Laske, G., and Masters, G. (1997). A global digital map of sediment thickness.*Eos Trans. AGU*, *78*(F483).

Laske, G., Masters, G., Ma, Z., and Pasyanos, M. (2013). Update on CRUST1. 0-A 1-degree global model of Earth's crust. In *Geophys. Res. Abstracts* (Vol. 15, p. 2658).

Lebedev, S., Adam, J. M. C., and Meier, T. (2013). Mapping the Moho with seismic surface waves: A review, resolution analysis, and recommended inversion strategies. Tectonophysics, 609, 377-394.

Mayer-Gürr, T., Rieser, D., Höck, E., Brockmann, J.M., Schuh, W.D., Krasbutter, I., Kusche, J., Maier, A., Krauss, S., Hausleitner, W. and Baur, O. (2012). The new combined satellite only model GOCO03s. *Abstract, GGHS2012, Venice*.

Meier, U., Curtis, A., and Trampert, J. (2007). Global crustal thickness from neural network inversion of surface wave data. *Geophysical Journal International*, *169*(2), 706-722.

Meinesz, F. A. V. (1931). Une nouvelle methode pour la reduction isostatique regionale de l'intensite de la pesanteur. *Bulletin Géodésique (1922-1941)*, *29*(1), 33-51.

Mooney, W. D. (2007). Crust and Lithospheric Structure – Global Crustal Structure. Treatise on Geophysics, vol. 1: Seismology and Structure of the Earth. (Eds. B. Romanowicz and A. Dziewonski). Elsevier, 361-417.

Moritz, H. (1990). The figure of the Earth, H Wichmann, Karlsruhe.

Pasyanos, M. E., and Nyblade, A. A. (2007). A top to bottom lithospheric study of Africa and Arabia. *Tectonophysics*, *444*(1), 27-44.

Pasyanos, M. E., Masters, G., Laske, G., and Ma, Z. (2012). LITHO1. 0-An Updated Crust and Lithospheric Model of the Earth Developed Using Multiple Data Constraints. In *AGU Fall Meeting Abstracts* (Vol. 1, p. 09).

Pavlis N. and Saleh J. (2004). Error propagation with geographic specificity for very high degree geopotential models, Presented at the IAG International symposium on gravity geoid and space missions 2004, Agust 30-September 3, Porto, Portugal.

Pratt, J. H. (1855). On the attraction of the Himalaya Mountains, and of the elevated regions beyond them, upon the plumb-line in India. *Philosophical Transactions of the Royal Society of London*, 53-100.

Reguzzoni, M., Sampietro, D., and Sansò, F. (2013). Global Moho from the combination of the CRUST2. 0 model and GOCE data. *Geophysical Journal International*, ggt247.

Reguzzoni, M., and Sampietro, D. (2015). GEMMA: An Earth crustal model based on GOCE satellite data. *International Journal of Applied Earth Observation and Geoinformation*, *35*, 31-43.

Rummel, R., Rapp, R. H., Suenkel, H., and Tscherning, C. C. (1988). Comparisons of global topographic/isostatic models to the Earth's observed gravity field.

Schuck, A., and Lange, G. (2007). Seismic methods. In *Environmental Geology* (pp. 337-402). Springer Berlin Heidelberg.

Shapiro, N. M., and Ritzwoller, M. H. (2002). Monte-Carlo inversion for a global shear-velocity model of the crust and upper mantle. *Geophysical Journal International*, *151*(1), 88-105.

Sjöberg, L. E. (2009). Solving Vening Meinesz-Moritz inverse problem in isostasy. *Geophysical Journal International*, *179*(3), 1527-1536.

Sjöberg, L. E., and Bagherbandi, M. (2011). A method of estimating the Moho density contrast with a tentative application of EGM08 and CRUST2.0. *Acta Geophysica*, *59*(3), 502-525.

Sjöberg, L. E. (2013). On the isostatic gravity anomaly and disturbance and their applications to Vening Meinesz–Moritz gravimetric inverse problem.*Geophysical Journal International*, ggt008.

Sjöberg, L. E. and Bagherbandi, M. (2014). Isostasy–Geodesy. In *Encyclopedia of* Geodesy. Springer International Publishing Switzerland 2014.

Sjöberg, L. E., Bagherbandi, M., and Tenzer, R. (2015). On Gravity Inversion by No-Topography and Rigorous Isostatic Gravity Anomalies. *Pure and Applied Geophysics*, 1-12.

Tenzer, R., Hamayun, K., and Vajda, P. (2009). Global maps of the CRUST 2.0 crustal components stripped gravity disturbances. *Journal of Geophysical Research: Solid Earth (1978–2012)*, *114*(B5).

Tenzer, R., and Bagherbandi, M. (2012). Reformulation of the Vening-Meinesz Moritz inverse problem of isostasy for isostatic gravity disturbances.*International Journal of Geosciences*, *3*(05), 918.

Tenzer, R., Pavel, N., and Vladislav, G. (2012). The bathymetric stripping corrections to gravity field quantities for a depth-dependent model of seawater density. *Marine Geodesy*, *35*(2), 198-220.

Tenzer, R., and Chen, W. (2014). Expressions for the global gravimetric Moho modeling in spectral domain. *Pure and Applied Geophysics*, *171*(8), 1877-1896.

Tenzer, R., Chen, W., Tsoulis, D., Bagherbandi, M., Sjöberg, L. E., Novák, P., and Jin, S. (2015a). Analysis of the refined CRUST1. 0 crustal model and its gravity field. *Surveys in geophysics*, *36*(1), 139-165.

Tenzer, R., Chen, W., and Jin, S. (2015b). Effect of Upper Mantle Density Structure on Moho Geometry. *Pure and Applied Geophysics*, *172*(6), 1563-1583.

Watts, A. B. (2001). Isostasy and Flexure of the Lithosphere. Cambridge University Press.

Watts, A.B. (2011). Encyclopedia of Solid Earth Geophysics.

# PART TWO

## Publications

**PAPER A:**

Abrehdary, M., Sjöberg, L.E., and Bagherbandi, M. (2015). Modelling Moho depth in ocean areas based on satellite altimetry using Vening Meinesz–Moritz' method, (Published in Journal of Acta Geodaetica et Geophysica, 1-13).

**PAPER B:**

Abrehdary, M., Sjöberg, L.E., and Bagherbandi, M. (2015). Combined Moho parameters determination using CRUST1.0 and Vening Meinesz-Moritz Model, (Published in Journal of Earth Science, 26(4), 607-616).

**PAPER C:**

Abrehdary, M., Sjöberg, L.E., and Bagherbandi, M. (2015). The spherical terrain correction and its effect on the gravimetric-isostatic Moho determination, (Published in Geophysical Journal International, 204(1), 262-273).

**PAPER D:**

Abrehdary, M., Sjöberg, L.E., Bagherbandi, M., and Sampietro D. (2015) Modelling Moho parameters and their uncertainties from the combination of the seismic and satellite gravity data, (Submitted to Journal of Geodesy).

**PAPER E:**

Bagherbandi, M., Sjöberg, L.E., Tenzer, R., and Abrehdary, M. (2015). A new Fennoscandian crustal thickness model based on CRUST1.0 and a gravimetric–isostatic approach, (Published in Journal of Earth-Science Reviews, 145, 132-145).

**PAPER F:**

Bagherbandi, M., Tenzer, R., Sjöberg, L.E., and Abrehdary, M. (2015). On the residual isostatic topography effect in the gravimetric Moho determination, (Published in Journal of Geodynamics, 83, 28-36).

**PAPER G:**

Bagherbandi, M., Sjöberg, L.E., Bai, Y., Tenzer, R., Abrehdary, M. Miranda, S., and Sanchez, J.M. (2016). Effect of the lithospheric thermal state on the Moho geometry, (Submitted to Journal of South American Earth Science).

**PAPER H:**

Sjöberg, L.E., Abrehdary, M., and Bagherbandi, M. (2014). The observed geoid height versus Airy's and Pratt's isostatic models using matched asymptotic expansions, (Published in Journal of Acta Geodaetica et Geophysica, 49(4), 473-490).